THE ASTROPHYSICAL JOURNAL, 450:593–615, 1995 September 10

NGC 7217: A SPHEROID-DOMINATED, EARLY-TYPE RESONANCE RING SPIRAL GALAXY

R. BUTA,[1] W. VAN DRIEL,[2,3] J. BRAINE,[4,5] F. COMBES,[4,6] K. WAKAMATSU,[7] Y. SOFUE,[8] AND A. TOMITA[9]

Received 1994 June 7; accepted 1995 March 21

ABSTRACT

NGC 7217 is a well-known northern spiral galaxy which is characterized by flocculent spiral structure and a series of three optical ringlike zones: a nuclear ring 21″ in diameter, a weak inner ring 63″ in diameter, and a striking outer ring 2.′6 in diameter. The rings all have nearly the same shape and position angle in projection. The appearance of the galaxy suggests that it may be more axisymmetric than the typical spiral galaxy, since there is little evidence for the presence of a bar, oval, or stellar density wave. This makes the origin of the ring features uncertain. In an effort to understand this kind of ringed galaxy, which is by no means typical, we have obtained multicolor CCD *BVRI* images, accurate surface photometry, mappings of the CO and H I gas distributions, and rotational velocities from Hα and H I spectral line data.

Our deep surface photometry has revealed an important feature of NGC 7217 that was missed in previous studies: The region occupied by the rings of the galaxy is surrounded by an extensive, nearly circular luminous halo. This halo cannot be merely an extension of the disk component because it is much rounder than the inner regions. Instead, we believe the light represents either the outer regions of the bulge or a separate stellar halo component. We are able to successfully model the luminosity profile in terms of an $r^{1/4}$ "spheroid" and an exponential disk with a spheroid-to-total disk (including rings) luminosity ratio of 2.3–2.4. This makes NGC 7217 one of the most spheroid-dominated spirals known, and the finding has important implications for the recent discovery by Merrifield and Kuijken of a significant population of counter-rotating stars in the galaxy.

Although the spiral structure of NGC 7217 is flocculent in blue light, there is a definite two-armed stellar spiral in the region of the outer ring. This ring includes about 4.4% of the total blue luminosity and is the locus of most of the recent star formation in the galaxy. The ring is also where we find the H I gas to be concentrated. The galaxy is very gas poor ($M_{\rm H\,I}/L_B^0 = 0.024\ M_\odot/L_{\odot,B}$) for its morphological type. The H I rotational velocities agree well with published and our new Hα-values.

Fourier analysis reveals a very weak possible oval distortion in the stellar mass distribution. Using the *I*-band light distribution to define the potential, we carried out simulations of gas streaming with no self-gravity. A model with a bulge-to-disk mass ratio of 2.4 reproduces the observed optical ring morphology very well. This suggests to us that in spite of the extreme weakness of the observed nonaxisymmetry of this galaxy, this nonaxisymmetry is still sufficient to torque the gas into the usual resonance rings identified in other, more obviously barred galaxies.

An additional noteworthy feature that we have identified in a $B-I$ color index map is a symmetric, nuclear *dust* ring 17″ in angular diameter. Other dust lanes are seen mainly on the near side of the galaxy.

Subject headings: galaxies: individual (NGC 7217) — galaxies: kinematics and dynamics — galaxies: photometry — galaxies: spiral — galaxies: structure

1. INTRODUCTION

The class of normal galaxies known as "ringed galaxies" has recently received a great deal of attention. The typical ringed galaxy has a bar or oval in the inner regions, and one, two, or three optical rings or pseudorings which neatly fit into the inner, outer, and nuclear ring categories that are recognized in classification systems (see, e.g., Sandage 1961; de Vaucouleurs 1959; Buta & Crocker 1991). The rings in these galaxies are well understood: most are likely to be "resonance" rings, regions where gas, moving in step with the pattern speed of the bar or oval, has been collected owing to gravity torques. The prototypical ringed barred galaxy is NGC 1433 (Buta 1986b), and many other examples are included in de Vaucouleurs & Buta (1980) and in the Catalog of Southern Ringed Galaxies (Buta 1991, 1995). It should be noted that some ringed galaxies classified as "nonbarred" may have prominent oval disks or may reveal a bar when imaged in near-infrared passbands.

In contrast to the "typical" ringed galaxy, NGC 7217 appears even on near-infrared photographs to have no clear bar or oval, making it a possible example of a mostly *axisymmetric* ringed galaxy. A ring can also involve a resonance with a strong global spiral density wave even when no bar is present. The pattern speed of the density wave (which could be excited by a companion) in such a case would determine the

[1] Department of Physics and Astronomy, University of Alabama, Box 870324, Tuscaloosa AL 35487-0324.
[2] Kiso Observatory, Institute of Astronomy, The University of Tokyo, Mitake-mura, Kiso-gun, Nagano-ken, 397-01 Japan.
[3] Station de Radioastronomie, Nancay, F-18330, Neuvy sur Barangeon, France.
[4] DEMIRM, Observatoire de Paris, Section de Meudon, 92195 Meudon Cedex, France.
[5] Max-Planck Institut für Radioastronomie, Auf dem Hügel 69, D-5300 Bonn 1, Germany.
[6] Radioastronomie Millimétrique, Laboratoire de Physique de l'Ecole Normale Supérieure, 24 Rue Lhomond, 75231 Paris, France.
[7] Department of Physics, College of Technology, Gifu University, Yanagido, Gifu-ken 501-11, Japan.
[8] Institute of Astronomy, The University of Tokyo, 2-21-1 Osawa, Mitaka, Tokyo 181, Japan.
[9] Department of Astronomy, Faculty of Science, Kyoto University, Sakyo-ku, Kyoto 606-01, Japan.

positions of the resonances. The spiral structure of NGC 7217 in blue light is, however, flocculent, so there seems to be no strong spiral density wave for the disk gas to resonate with. Nevertheless, the galaxy has three optical rings of similar shape and position angle. There is also evidence for nuclear activity in the galaxy, since it has a LINER spectrum, a nuclear Hα source, and a relatively strong nuclear radio source. The questions we ask are the following: (1) given the apparent lack of significant nonaxisymmetry, why does NGC 7217 have prominent rings? (2) What is the nature of these ring patterns compared to the more typical "resonance" rings?

NGC 7217 is also interesting for another reason. Merrifield & Kuijken (1994; see also Kuijken 1993) discovered a substantial population (up to 30%) of stars in NGC 7217 that are counter-rotating with respect to the majority of the stars. This was deduced from an analysis of absorption line profiles. Along the major axis, the velocities out to 30″ radius show a long tail away from the maximum rotation velocity which crosses the systemic velocity. Based on previously published surface photometry, Merrifield and Kuijken believe that the counter-rotating stars are disk stars, and suggest that the galaxy is similar to the case of NGC 4550, recently found to have two cospatial equally populated counter-rotating stellar disks (Rubin, Graham, & Kenney 1992). An uncertainty in the Merrifield and Kuijken analysis is the contribution of the bulge to the line profiles. We will show here that the bulge, or more appropriately the bulge/stellar halo, in NGC 7217 is much more significant than previous photometry had suggested.

In this paper we present a detailed analysis of broadband optical CCD images, 21 cm H I line radio synthesis observations, single-dish CO(1–0) and CO(2–1) line observations, and Hα observations of NGC 7217. We also present mass models deduced from the *I*-band light distribution in conjunction with the measured rotation curve. From these observations and other information, we find that NGC 7217 is a strongly bulge-dominated galaxy, poor in H I gas, and that the rings are likely to be resonances with a very weak oval distortion that can only be extracted from Fourier analysis.

The distance to NGC 7217 is best derived from the Tully-Fisher relation. Using 21 cm line widths W_{20} and W_{50} from RC3 (de Vaucouleurs et al. 1991), the total magnitude from this paper, and the procedures outlined by Bottinelli et al. (1980b, 1983), we derive a distance $\Delta = 14.5$ Mpc. Note that all radial velocities in this paper are heliocentric and calculated according to the conventional optical definition ($V = c\Delta\lambda/\lambda_0$). All coordinates given are for epoch 1950.0. Blue luminosities are expressed in units of the solar blue luminosity $L_{\odot,B}$ based on an absolute blue solar magnitude of 5.46 (see introduction to RC3).

In the next sections (2–5) we will discuss the optical CCD imaging observations and surface photometry of NGC 7217. We present the 21 cm H I line radio synthesis observations in § 6, the CO line observations in § 7, and the Hα observations in § 8. Mass models and gas simulations are presented in § 9, and results are discussed in § 10. Conclusions are presented in § 11.

2. CCD IMAGING, MORPHOLOGY, AND LOCAL ENVIRONMENT

Optical images of NGC 7217 were obtained in 1991 June with the ST1K 1024 square CCD attached to the Kitt Peak 0.9 m telescope. This chip has a read noise of 2.8 electrons, and the observations were made with a gain of 1.8 electrons per ADU. Total integration times of 1436, 840, and 600 s were obtained in *B*, *V*, and *I*, respectively. The images cover a field 10.′2 square, and all processing was accomplished using routines in IRAF. The pixel size is 0.″598 square. The observations were made under photometric conditions and were calibrated using standard stars from Landolt (1992). The *I*-band observations are in the Cousins system. To evaluate the uncertainties in the color and magnitude measurements we have simulated aperture photometry and compared the results to published photoelectric photometry in Longo & de Vaucouleurs (1983) and in de Vaucouleurs & Longo (1988). The mean differences found (in the sense photoelectric minus CCD values) were $\langle \Delta V \rangle = +0.045 \pm 0.018$ ($n = 7$ observations), $\langle \Delta B \rangle = +0.034 \pm 0.024$ ($n = 7$), $\langle \Delta(B-V) \rangle = -0.011 \pm 0.022$ ($n = 7$), and $\langle \Delta(V-I) \rangle = +0.016$ ($n = 1$). The differences are satisfactorily small, and especially indicate that our color measurements are reliable.

Additional images were obtained with the 1.05 m Kiso Schmidt telescope. The liquid nitrogen-cooled TC-215 CCD chip used has an effective imaging area of 1000 × 1018 pixels of 0.″75 square each, giving a field of view of 12.′5 × 12.′7 ($\Delta\alpha \times \Delta\delta$). The read noise is 14 electrons and the gain used was about 1 electron per ADU. Images were taken in *V* and *R* only, and for each filter we obtained 1^m, 5^m, and 30^m exposures. The latter were very saturated in the center. Since no standard stars were obtained, we computed zero points for these images by bootstrapping the long and short exposures and using the available published aperture photometry. Standard bias subtraction and flat-fielding were also performed with the IRAF software package.

The morphology of NGC 7217 is illustrated in Figures 1–3 (Plates 25–27; see also Table 1). Figure 1 presents a *B*-band image printed to show the bright inner disk region. The image is logarithmic and has been converted to units of mag

TABLE 1

GLOBAL OPTICAL CHARACTERISTICS OF NGC 7217

Parameter	Value
α(1950)	$22^h05^m37^s.8$
δ(1950)	+31°06′51″
RC3 type[a]	(R)SA(r)ab
RSA type[b]	Sb(r) II–III
Refined type[c]	(R′)SA(rs, nr)ab
B_T	10.95 ± 0.04
M_T^0 (T-F relation)	−20.5
$(B-V)_T$	0.92
$(V-I)_T$	1.35
$(B-V)_e$	0.99
$(V-I)_e$	1.36
log A_e (0.′1)	1.23 ± 0.03
log D_{25} (0.′1)	1.643
log R_{25}	0.025
Disk axis ratio	0.83 ± 0.01
Spheroid axis ratio	0.96 ± 0.01
Inclination[d]	35°
Disk major axis position angle	91° ± 1°
Spheroid major axis position angle	91° ± 7°

[a] de Vaucouleurs et al. 1991. The (r) referred to in this type is what we call the stellar nuclear ring in this paper (see de Vaucouleurs & Buta 1980).

[b] Sandage & Tammann (1981).

[c] This type allows for all three ring features discussed in the text.

[d] Based on disk axis ratio of 0.83 and eqs. (1) and (2) of Bottinelli et al. 1983.

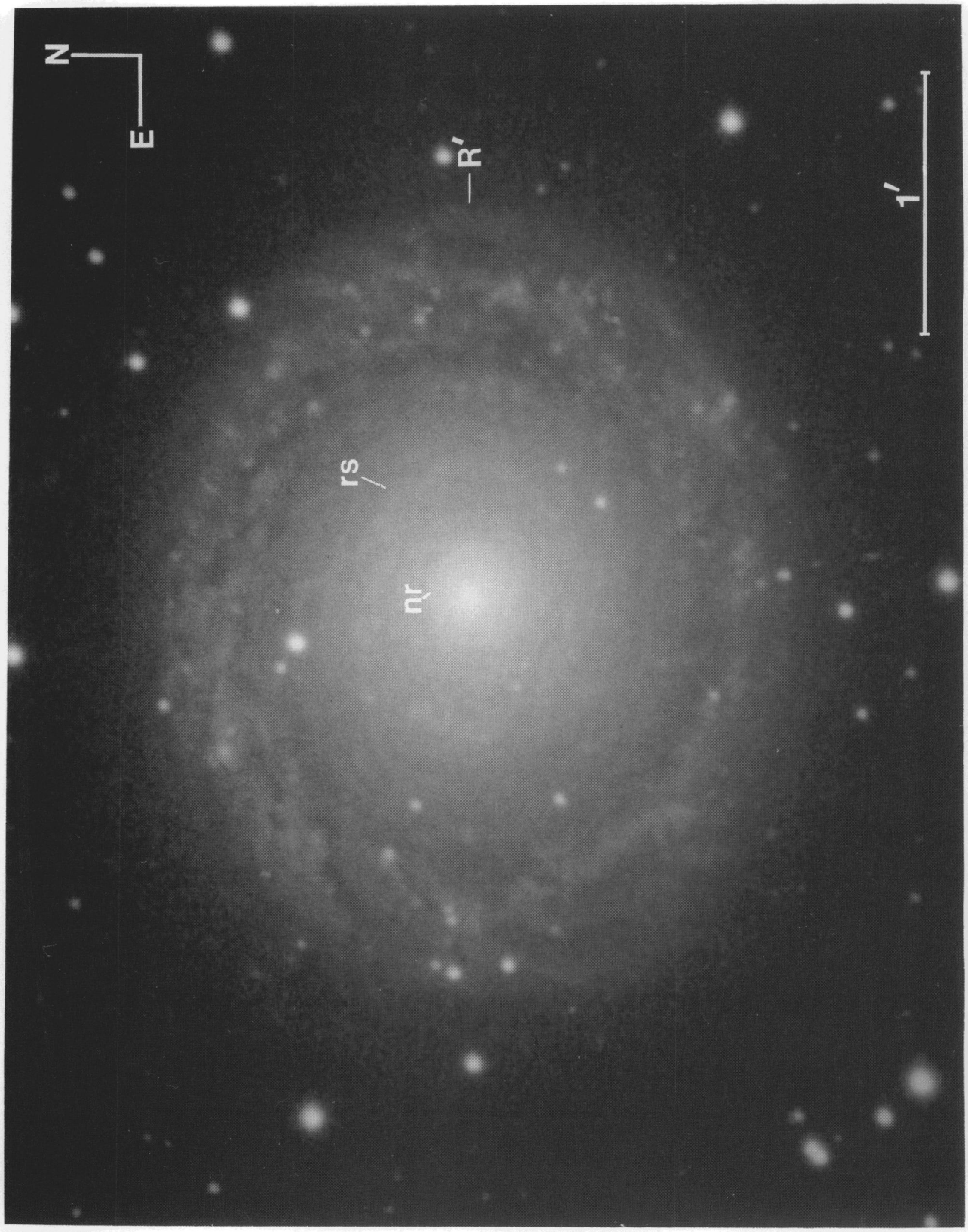

FIG. 1.—*B*-band CCD image of NGC 7217, printed to show the inner disk structure. The units of the image are mag arcsec^{-2} in the range 18.0–28.0.

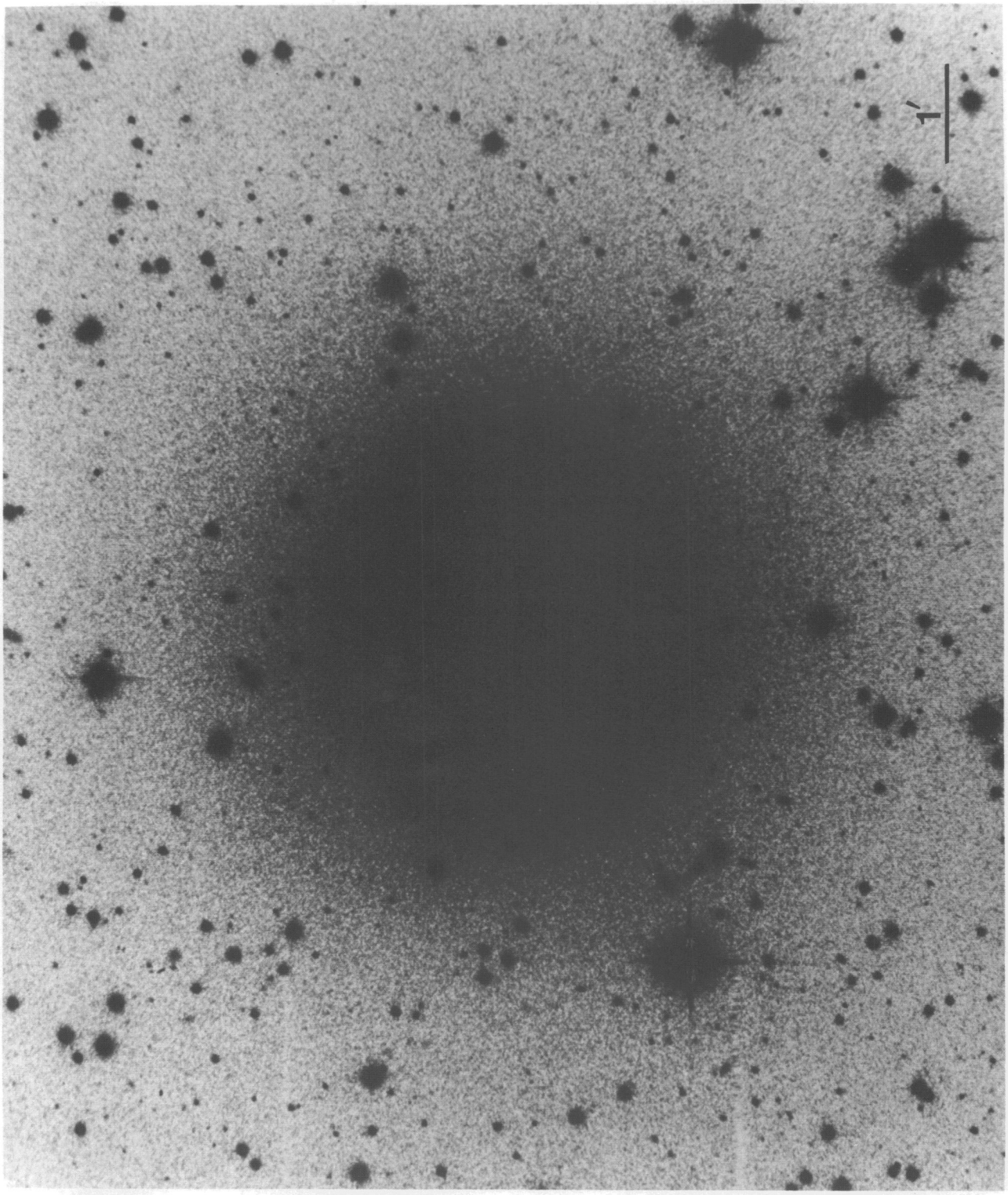

FIG. 2.—*B*-band CCD image of NGC 7217, printed to show the extended, nearly round stellar halo. Units and orientation are the same as in Fig. 1.

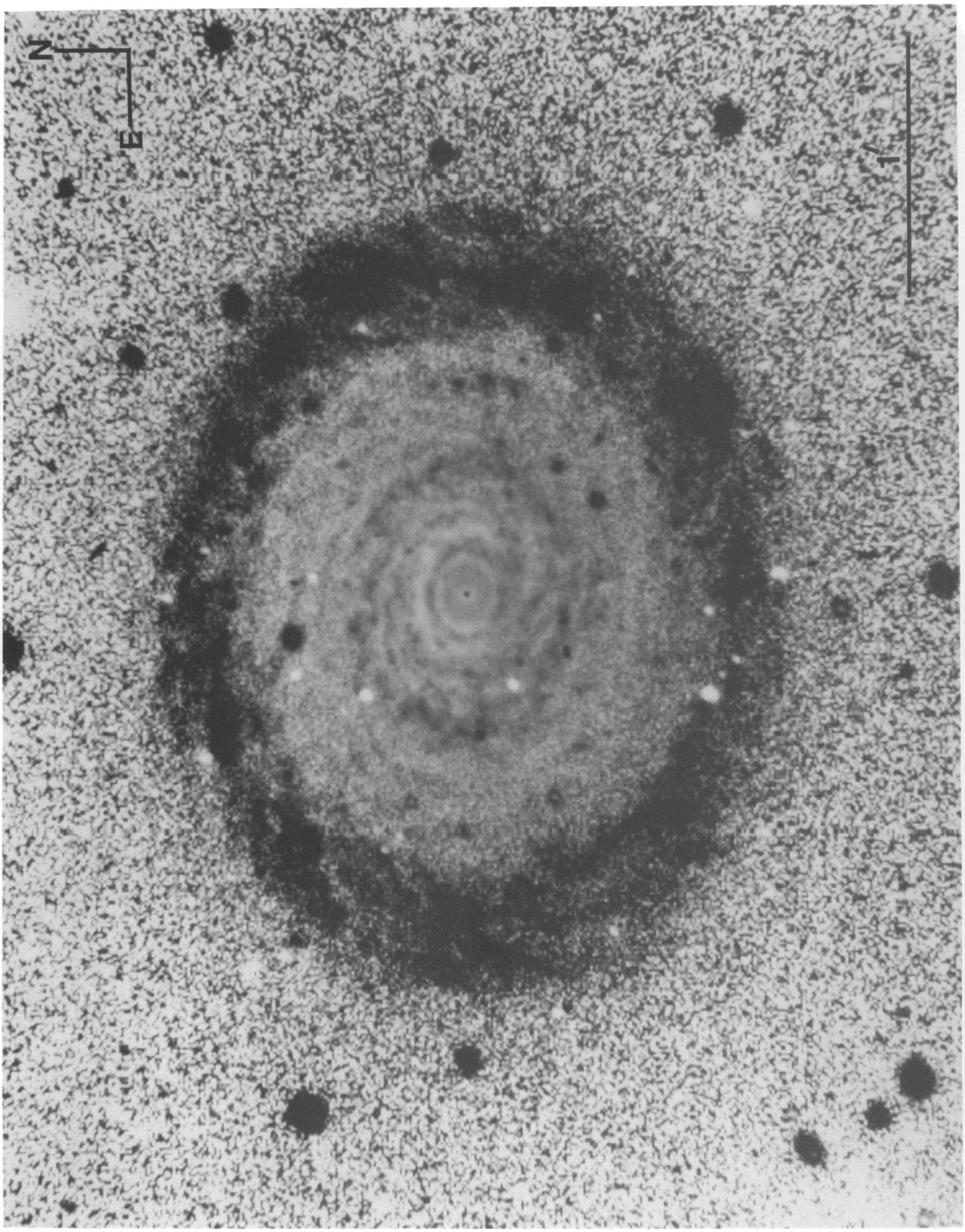

FIG. 3.—$B-I$ color index map of NGC 7217. The gray scale is such that blue pixels ($B-I \approx 1$) are dark and red pixels ($B-I \approx 3$) are light. Note spectacular concentration of star-forming sites in the outer ring. The central few pixels are not reliable due to slight core saturation in the I-band image.

TABLE 2

RING DIAMETERS AND AXIS RATIOS

Feature	Apparent Diameter	Axis Ratio	Linear Diameter[a] (kpc)
Outer ring	154".0	0.83	10.8
Inner ring	63.2	0.83	4.4
Stellar nuclear ring	21.4	0.78	1.5
Hα + [N II] nuclear ring[b]	21.7:	0.79	1.5
Nuclear dust ring	17.2	0.78	1.2

[a] For $\Delta = 14.5$ Mpc, based on the Tully-Fisher relation derived by Bottinelli et al. 1980.
[b] See Fig. 16 of Pogge 1989; these visual measurements are based on that image.

arcsec^{-2}, the range being from 18.0 to 28.0 mag arcsec^{-2}. The three ring features are labeled, where nr refers to nuclear ring, rs refers to inner ring, and R′ refers to outer ring. The apparent diameters and axis ratios, as well as linear diameters, of these features are summarized in Table 2. Figure 1 illustrates how the nuclear ring is a closed oval feature, while the inner and outer rings are defined by flocculent spiral structure and hence are better characterized as pseudorings. In Figure 2, we see a feature that is completely invisible in the print of NGC 7217 in the Hubble Atlas (Sandage 1961): beyond the outer ring there is an extended halo that is rounder in apparent shape than the inner disk. Our analysis in § 4 suggests that this light is dominated by the spheroidal component of the galaxy, which is nearly spherical. The extended light nearly fills the fields of our CCD arrays and complicates the sky subtraction.

In Figure 3 we display a $B-I$ color index map of the whole disk region. This map is coded such that blue pixels ($B-I \approx 1.0$) are dark and red pixels ($B-I \approx 2.5$) are light. (A few pixels near the center in this image appear blue because of slight saturation in the I-band image). The following features are revealed in this map: (1) The outer ring is a sharply bounded zone of recent star formation. The width of the star-forming zone is nearly 40″ (2.8 kpc), and it lies in the radius range $60'' < r < 100''$. (2) The inner ring is also a zone of slightly bluer colors, but it is much narrower in extent. In the region between the nuclear and inner rings we see a mixture of slightly blue flocculent spiral structure and dust lanes. The greater prominence of the dust lanes on the north side indicates that this is the near side of the galaxy (see de Vaucouleurs 1958). Using the rotation data of Peterson et al. (1978), which is confirmed by our own data, we deduce that the spiral structure is trailing. (3) Near the center we see what appears to be a closed symmetric ring of dust. It turns out that this feature does *not* coincide with the bright nuclear ring in the B-band image. To illustrate this feature better, we display in Figures 4 and 5 (Plates 28 and 29) close-up views of the B and $B-I$ distributions. The nuclear dust ring apparently defines the sharp inner edge of the stellar nuclear ring. It is not clear that the stellar nuclear ring is defined entirely by dust. However, it is noteworthy that the region of the stellar nuclear ring is not a strong blue enhancement. These findings can be compared with Hα + [N II] observations of the central few arcminutes of NGC 7217 published by Pogge (1989). His continuum-subtracted image reveals bright central emission and a circumnuclear ring about 21".7 in diameter. Within the uncertainties, this gas ring coincides with the apparent stellar nuclear ring, not the dust ring.

It is also noteworthy that NGC 7217 is entered in the Catalogue of Isolated Galaxies (Karachentseva 1973). This isolation means we can study the features observed from the point of view of internal dynamics alone.

3. SURFACE PHOTOMETRY

Surface photometry of NGC 7217 has been published by Boroson (1981) and Kent (1986) out to radii of 141″ and 106″, respectively. Boroson derived a bulge-to-disk luminosity ratio of 0.39 (bulge-to-total ratio = 0.28) from an $r^{1/4}$ fit to inner surface brightnesses. Kent (1986) used an iterative bulge/disk decomposition that makes no assumptions about the form of the components, and estimated a bulge-to-disk luminosity ratio of 1:3 for the galaxy. However, in neither of these studies does the photometry include the extensive outer halo. Thus, the decompositions presented by Kent and Boroson probably overestimate the disk contribution significantly. Our analysis reveals a much more significant bulge or spheroid in NGC 7217.

Analysis of the images was accomplished using standard routines in IRAF. Flat-fielding and bias pattern removal were good for the KPNO BV and Kiso VR images, but the flat-fielding was poorer for the KPNO I-band image. Thus, the sky level is more uncertain for the latter image compared to the others. The IRAF routines DAOFIND, PHOT, PSF, PEAK, and SUBSTAR were used to remove many of the fainter stars in the images. This uses the method described by Stetson (1987) whereby a model of the point spread function is made, and this function is fitted either singly or multiply to each star found by DAOFIND. For a large number of stars in the field, this approach worked very well. If SUBSTAR left noticeable residuals near the center of the star, we used a program written by W. D. Pence that fits a low-order polynomial to surrounding background intensities and interpolates this polynomial across the area of a specified "patch." However, for the brighter stars, this method was ineffective because the required patch sizes were too large. In these cases, we simply "blanked out" the largest area possible and did not use the pixels in those areas in some of our analysis.

Since NGC 7217 is largely axisymmetric, it is an ideal case for deriving an "ellipse fit" luminosity profile, which is obtained by fitting ellipses to the isophotes at varying surface brightness levels. We solve for the coordinates of the center, the major axis and minor axis radii, and the major axis position angle using linear least squares. The approach differs from that of Cawson (1983; see Davis et al. 1985 and Cornell et al. 1987), in that we choose surface brightness levels (mag arcsec^{-2}) and find the best-fitting radius, whereas Cawson's program chooses radii and provides the best-fitting surface brightness. Either method gives an "ellipse fit" profile, whose advantage is that it uses the whole two-dimensional image and consequently has a

PLATE 28

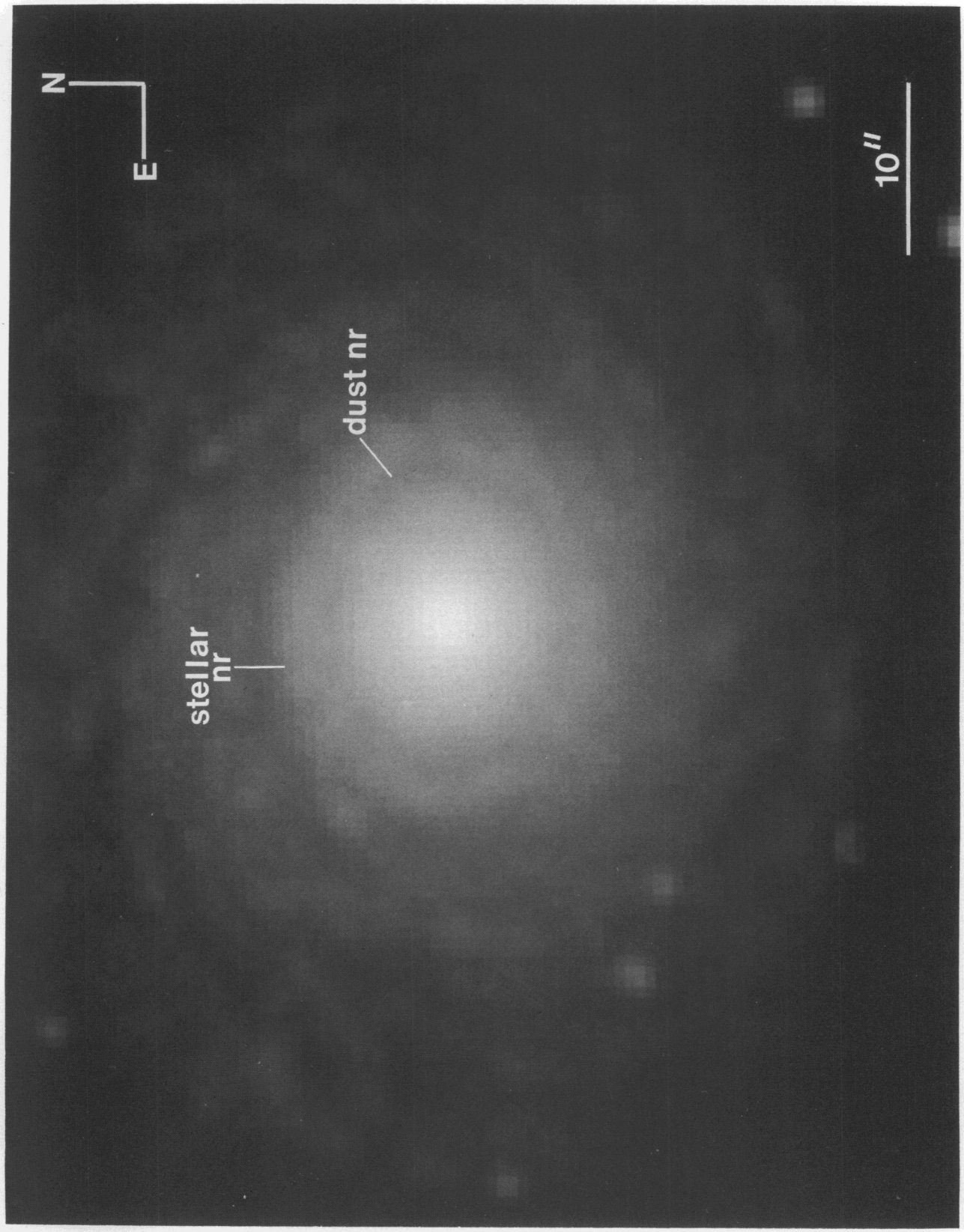

FIG. 4.—Enlargement of the central regions of NGC 7217 in the *B* band. The stellar nuclear ring and the dust nuclear ring are labeled. The units of the image are the same as in Fig. 1.

1995ApJ...450..593B

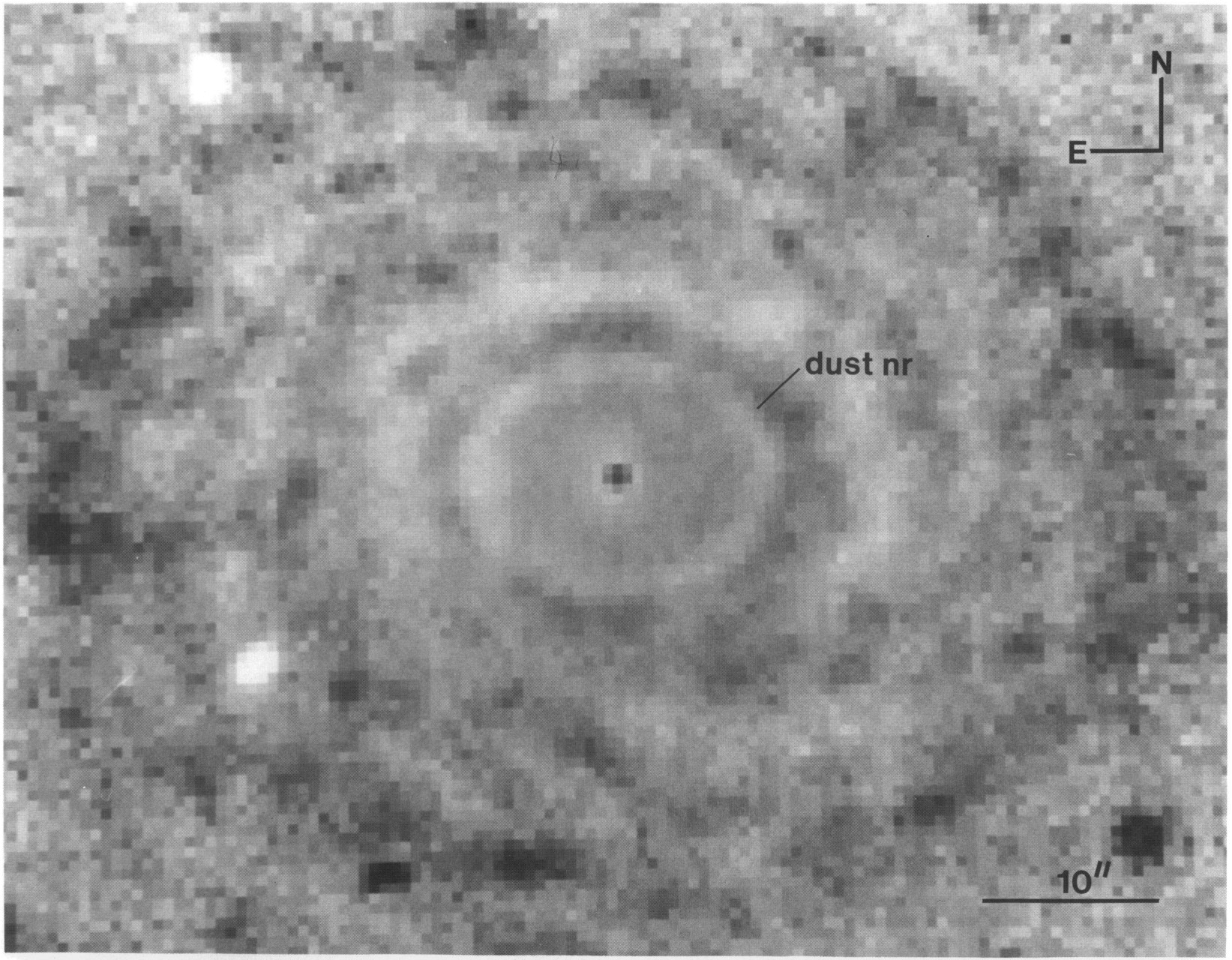

FIG. 5.—Enlargement of the central regions of NGC 7217 in $B-I$, showing the inner dust patterns, including the nuclear dust ring. The gray-scale coding is the same as in Fig. 3. The central few pixels are not reliable due to slight core saturation in the I-band image. Mean $\mu_B - \mu_V$, $\mu_V - \mu_I$, and $\mu_B - \mu_I$ colors of features are as follows: nuclear dust ring—1.04, 1.39, 2.43; stellar nuclear ring—0.97, 1.36, 2.33; and prominent dust lane on outer edge of stellar nuclear ring—1.05, 1.45, 2.50.

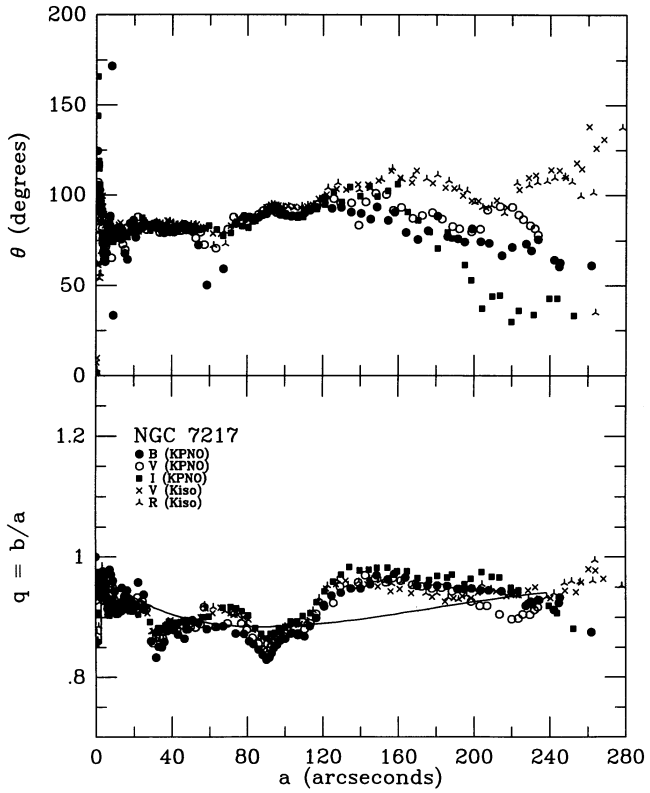

FIG. 6.—Variation of the axis ratio (q) and major axis position angle (θ) of isophotes as a function of major axis radius a, based on ellipse fits. The different filters are indicated.

high signal-to-noise ratio over profiles interpolated just along the major axis. Like Cawson, we blank out patches occupied by bright stars from the fits. The advantage of our approach over Cawson's is that we do not need initial guesses of the parameters; the disadvantage is that we must interpolate the profiles in different filters to the same radii if we want color index profiles. We note that the isophotes at large radii were fitted using binned arrays ranging from bins of 2 × 2 to 8 × 8 pixels from the original arrays.

The results of the ellipse fits are displayed in Figures 6–9. In Figure 6, we show the fitted axis ratio $q = b/a$ and major axis position angle θ of the ellipses (for 0.1 mag arcsec^{-2} steps in surface brightness) as a function of the fitted major axis radius a. Different symbols are used for the different filters and telescopes. The minimum axis ratio achieved is 0.83 in B at $a = 90''$, which nearly coincides with the outermost boundary of the outer ring. This axis ratio is identical to that for the ridge line of the outer ring (Table 2) and may closely approximate the apparent disk axis ratio if the ring is intrinsically nearly circular. Beyond, $a = 90''$, the axis ratio increases to 0.96 in all filters, and then appears to decrease slightly past $a = 160''$. Although most of the filters are in agreement on this decrease, we cannot be certain of its reality due to the influence of bright field stars, particularly the one located 195″ to the southeast (see Fig. 2).

The position angles are relatively constant at $\theta_o = 91°$ in the range $90'' < a < 120''$. Thereafter, the scatter is too large for a reliable judgment (mostly because the isophotes are so nearly circular) and the different filters indicate that 91° could be taken as the major axis position angle of the whole galaxy. The larger axis ratio of isophotes of the outer regions suggests that the light out here is not part of the disk component. There are two possible interpretations. One is that the light is merely the extension of the central bulge, and that the galaxy has a relatively minor disk component embedded in a dominating bulge component. A second interpretation is that the outer light really defines a true stellar halo like that in the Milky Way. The only way to make the distinction would be to study the metallicity and rotation characteristics of the inner and outer regions. Lacking this information, we will call the bulge plus halo the "spheroid" and treat it initially as a single component. We therefore take 0.96 to be the apparent flattening of the spheroid, and will evaluate the idea using photometric decomposition in the next section.

The KPNO and Kiso ellipse fit luminosity and color profiles are illustrated in Figure 7 (see also Tables 3 and 4); the computation of the error bars is discussed in the Appendix. The only filter in common between the two sets of images is the V band, and Figure 7 shows both V-band profiles with different

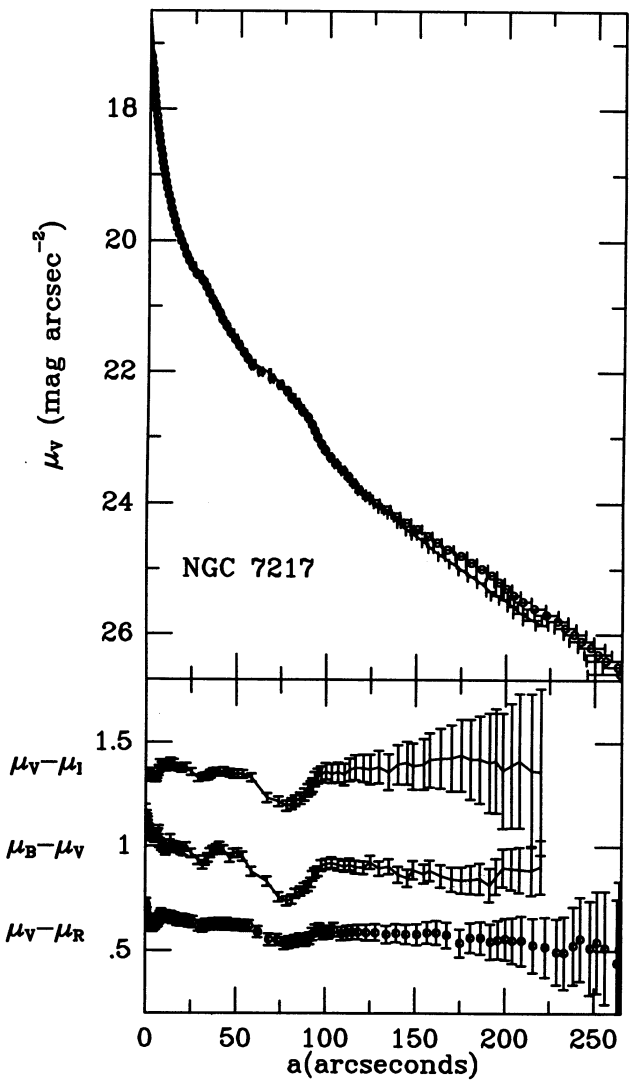

FIG. 7. Luminosity and color index profiles of NGC 7217 based on ellipse fits. Solid curves show KPNO data, while the open circles show Kiso data. The error bars are discussed in the Appendix.

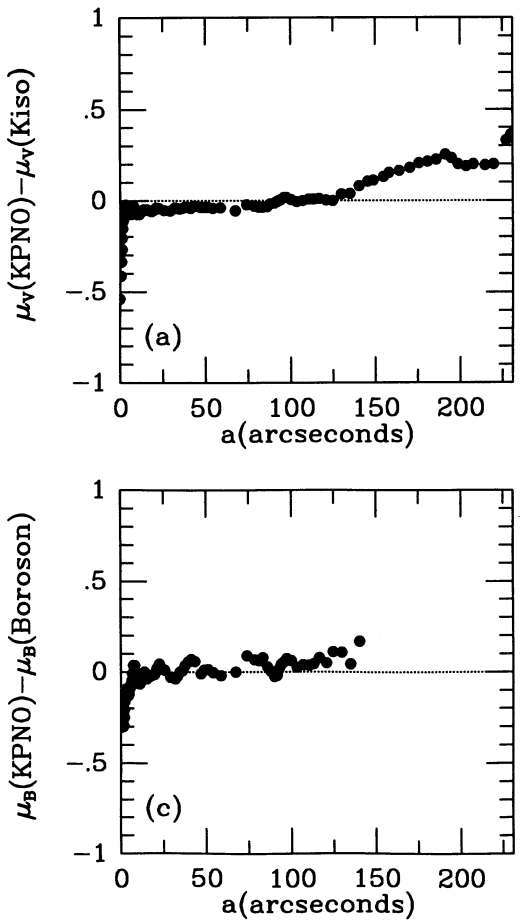

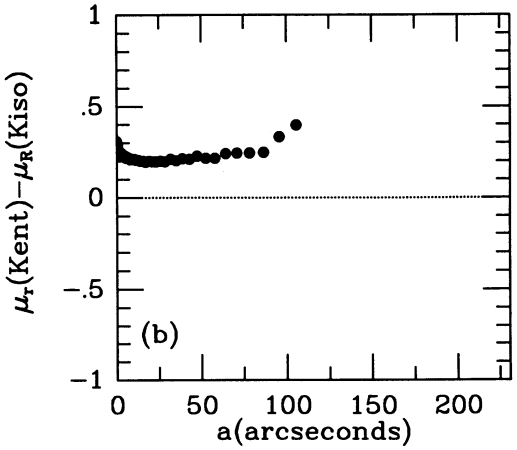

FIG. 8.—Comparison of KPNO and Kiso ellipse-fit luminosity profiles with each other and with similar data from Boroson (1981) and Kent (1986).

symbols. There is very good agreement for $a < 130''$, but at larger radii the Kiso surface brightnesses are slightly brighter than the KPNO surface brightnesses by a few tenths of a magnitude. A more detailed comparison is shown in Figure 8*a*, which plots the difference between the profiles as a function of radius. There is a small zero-point difference (≈ 0.04 mag) for $r < 50''$ that is due to the differences in the calibrations of the images: KPNO with standard stars and Kiso with photoelectric aperture photometry. The agreement in profile shapes is very good for $a < 90''$, but thereafter the profiles differ systematically. The maximum difference achieved is 0.39 mag arcsec^{-2} (relative to the inner difference) at $a = 230''$. Although some of this difference could be explained by simple sky-subtraction uncertainties, we believe it is mostly due to uncertainties in the flat-fielding and possibly also to problems associated with the very bright field stars. The star located 195″ to the southeast is very bright and has large spikes and a halo on both Kiso images. It was difficult to remove the effect of this star entirely. Other bright stars to the southwest further complicated the photometry at large radii.

The previously published surface photometry of Boroson (1981) and Kent (1986) cannot resolve the discrepancy between the KPNO and Kiso profiles, but still can provide a useful external check on our new photometry. The profiles of these authors are similar ellipse average or ellipse fit types, and are directly comparable to our profiles. Figure 8*b* compares the Kiso *R*-band profile with the photographic IIIa-F profile of Kent (1986). The agreement is very good to a radius of 87″. The zero-point difference of ≈ 0.2 mag is due to the transformations used: our profile is in the Kron-Cousins *R* system, while Kent's was transformed to the Thuan-Gunn *r* system. The comparison between the *B*-band profile of Boroson (1981) and the KPNO *B*-band profile is shown in Figure 8*c*. Again, the agreement is fairly good, except for the central few arcseconds, over the full range available for comparison. These results are consistent with independent findings by Whitmore & Kirschner (1982) for several other galaxies in Boroson's sample. (The computational error in Boroson's profiles discussed by Whitmore & Kirschner 1982 is not very serious for this galaxy since the inclination is low.)

The color profiles in Figure 7 are dominated by the large dip at the location of the outer ring. The dip is significant in all of the color indices. Just inside the ring, the ellipse fit color is $B-I = 2.30$, while just outside the color is $B-I = 2.27$. At the bluest part, the ellipse fit color is $B-I = 1.93$, a drop of 0.36 mag arcsec^{-2}.

Table 1 summarizes some of the basic parameters that can be derived from the surface photometry. The total magnitude B_T, total colors $(B-V)_T$ and $(V-I)_T$, effective (or half power) aperture A_e, and the integrated colors $(B-V)_e$ and $(V-I)_e$ within this aperture are based on simulated circular aperture photometry. We fitted a standard "growth curve" (see RC3) to extrapolate the observed integrated fluxes to a well-defined total magnitude. The curve for type S0/a best fits the data for NGC 7217 in the largest apertures, and gave $B_T = 10.95$. Using the 21 cm line widths in RC3, and a compromise disk inclination of 35° from Table 1, the Tully-Fisher relation of Bottinelli et al. (1980b, 1983) yields $M_T^o(B) = -20.47$. Thus, NGC 7217 is a high-luminosity system, with $L_B = 2.4 \times 10^{10}$ $L_B(\odot)$.[10] Note that if we do not attribute the outer halo light to the spheroid, but instead consider it as part of the flattened disk, then the axis ratio of 0.96 would lead to an inclination of only 16°.6 (from eqs. [1] and [2] of Bottinelli et al. 1983) and *the maximum rotation velocity judged from the* 21 cm *line widths would be* 527 km s^{-1}. This would exceed that found for

[10] This value had to be based on the galactic extinction and inclination corrections from the Second Reference Catalogue of Bright Galaxies (RC2; de Vaucouleurs, de Vaucouleurs, & Corwin 1976), because the Bottinelli et al. calibration is based on these corrections. The corrected total magnitude of NGC 7217 in the RC2 system is $B_T^o = 10.34$, while in the RC3 system it is 10.40.

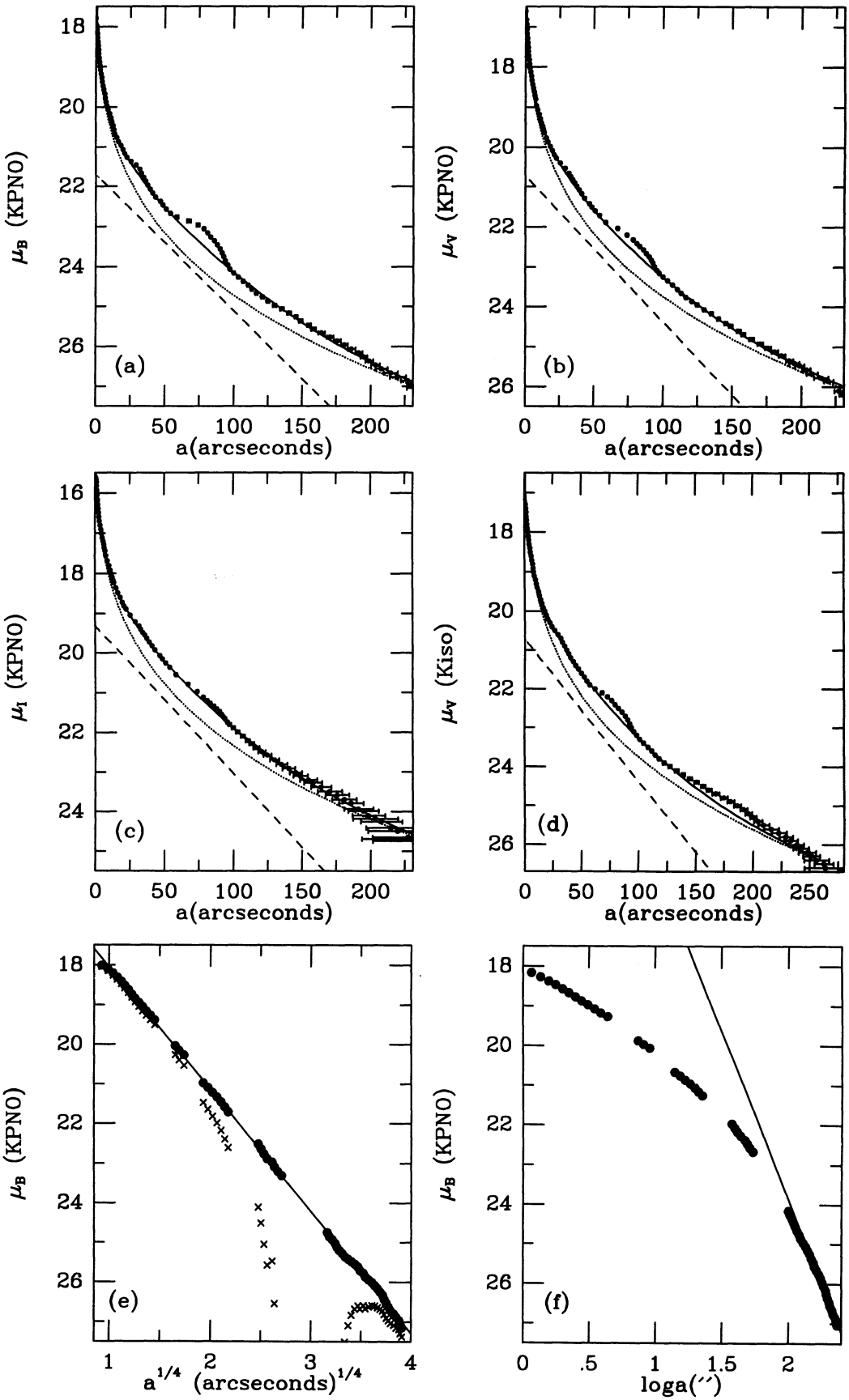

FIG. 9.—Results of bulge/disk/halo decompositions of the KPNO ellipse-fit profiles. The points are the data, while the dashed line is the disk model, the dotted line is the spheroid model, and the solid curve is the combined spheroid plus disk model. The curves shown in (*d*) are the same as in (*b*). In (*e*) we show the effect on the bulge surface brightnesses of forcing the disk to be dominant in the inner regions (*crosses*) as compared to the spheroid model in Table 5. Making the disk dominant would force both the bulge and the disk to truncate in an artificial way. In (*f*) we show a power-law fit to the surface brightnesses in the halo-dominated region beyond 140″ radius, and how this does not extrapolate well into the inner regions.

TABLE 3

KPNO Ellipse Fit Luminosity and Color Profiles[a]

a	μ_B	σ	$\mu_B-\mu_V$	σ	$\mu_V-\mu_I$	σ	a	μ_B	σ	$\mu_B-\mu_V$	σ	$\mu_V-\mu_I$	σ
0.00	17.79	0.02	1.18	0.02	–	–	51.05	22.57	0.02	0.97	0.02	1.35	0.02
0.75	17.97	0.02	1.15	0.02	–	–	54.07	22.66	0.02	0.95	0.02	1.35	0.02
0.96	18.07	0.02	1.13	0.02	–	–	58.69	22.76	0.02	0.88	0.02	1.33	0.02
1.16	18.17	0.02	1.12	0.02	1.33	0.02	67.36	22.86	0.02	0.83	0.02	1.23	0.02
1.37	18.27	0.02	1.10	0.02	1.35	0.02	74.01	22.95	0.02	0.76	0.02	1.22	0.02
1.57	18.37	0.02	1.09	0.02	1.35	0.02	78.34	23.05	0.02	0.74	0.02	1.19	0.02
1.78	18.47	0.02	1.07	0.02	1.34	0.02	81.11	23.15	0.02	0.75	0.02	1.20	0.03
2.00	18.57	0.02	1.06	0.02	1.34	0.02	83.35	23.26	0.02	0.77	0.02	1.22	0.03
2.25	18.67	0.02	1.06	0.02	1.33	0.02	86.07	23.36	0.02	0.78	0.02	1.23	0.03
2.51	18.77	0.02	1.05	0.02	1.33	0.02	88.18	23.46	0.02	0.80	0.02	1.25	0.03
2.80	18.87	0.02	1.05	0.02	1.33	0.02	90.29	23.56	0.02	0.81	0.02	1.27	0.03
3.12	18.97	0.02	1.05	0.02	1.33	0.02	91.82	23.66	0.02	0.83	0.02	1.28	0.03
3.49	19.07	0.02	1.04	0.02	1.33	0.02	92.92	23.76	0.02	0.86	0.02	1.29	0.03
3.91	19.17	0.02	1.05	0.02	1.32	0.02	94.22	23.86	0.02	0.87	0.02	1.32	0.03
4.42	19.27	0.02	1.05	0.02	1.32	0.02	95.84	23.96	0.02	0.88	0.02	1.34	0.04
4.99	19.37	0.02	1.04	0.02	1.32	0.02	97.51	24.06	0.02	0.91	0.02	1.34	0.04
5.54	19.47	0.02	1.04	0.02	1.32	0.02	100.22	24.16	0.02	0.91	0.03	1.36	0.04
6.07	19.57	0.02	1.05	0.02	1.33	0.02	103.28	24.26	0.02	0.92	0.03	1.35	0.04
6.58	19.67	0.02	1.05	0.02	1.34	0.02	106.92	24.36	0.02	0.91	0.03	1.35	0.05
7.04	19.77	0.02	1.06	0.02	1.35	0.02	110.52	24.46	0.02	0.90	0.03	1.34	0.05
7.44	19.87	0.02	1.08	0.02	1.37	0.02	113.31	24.56	0.02	0.91	0.03	1.37	0.06
8.18	19.97	0.02	1.01	0.02	1.40	0.02	116.76	24.66	0.02	0.90	0.03	1.38	0.06
9.11	20.07	0.02	1.00	0.02	1.38	0.02	120.97	24.76	0.02	0.90	0.03	1.38	0.07
10.19	20.17	0.02	0.99	0.02	1.37	0.02	124.81	24.86	0.03	0.92	0.03	1.37	0.07
11.19	20.27	0.02	0.98	0.02	1.37	0.02	129.82	24.96	0.03	0.89	0.03	1.38	0.08
11.86	20.37	0.02	0.99	0.02	1.38	0.02	135.09	25.06	0.03	0.90	0.04	1.36	0.09
12.64	20.47	0.02	0.99	0.02	1.39	0.02	140.31	25.16	0.03	0.86	0.04	1.39	0.09
13.33	20.57	0.02	1.01	0.02	1.39	0.02	145.44	25.26	0.03	0.85	0.04	1.40	0.10
13.97	20.67	0.02	1.03	0.02	1.40	0.02	148.87	25.36	0.03	0.89	0.04	1.39	0.11
15.34	20.77	0.02	1.00	0.02	1.40	0.02	154.74	25.46	0.03	0.87	0.05	1.40	0.12
16.71	20.87	0.02	1.00	0.02	1.38	0.02	158.10	25.56	0.04	0.88	0.05	1.41	0.13
18.32	20.97	0.02	0.99	0.02	1.38	0.02	164.10	25.66	0.04	0.86	0.05	1.42	0.14
19.79	21.07	0.02	0.98	0.02	1.37	0.02	170.37	25.76	0.04	0.84	0.06	1.42	0.16
21.12	21.17	0.02	0.97	0.02	1.38	0.02	175.84	25.86	0.05	0.84	0.06	1.44	0.17
22.53	21.27	0.02	0.99	0.02	1.38	0.02	180.94	25.96	0.05	0.84	0.07	1.42	0.19
25.45	21.37	0.02	0.97	0.02	1.36	0.02	186.11	26.06	0.05	0.85	0.07	1.42	0.21
29.15	21.46	0.02	0.93	0.02	1.33	0.02	191.54	26.16	0.06	0.82	0.08	1.40	0.24
31.76	21.56	0.02	0.91	0.02	1.33	0.02	195.07	26.26	0.06	0.86	0.09	1.41	0.25
33.16	21.66	0.02	0.93	0.02	1.33	0.02	198.99	26.36	0.07	0.90	0.09	1.36	0.28
34.71	21.76	0.02	0.94	0.02	1.34	0.02	203.65	26.46	0.07	0.89	0.10	1.39	0.30
36.07	21.87	0.02	0.97	0.02	1.35	0.02	207.99	26.56	0.08	0.89	0.11	1.41	0.32
37.61	21.97	0.02	0.98	0.02	1.35	0.02	214.81	26.66	0.09	0.88	0.12	1.36	0.37
39.38	22.07	0.02	0.99	0.02	1.36	0.02	220.06	26.76	0.09	0.90	0.13	1.36	0.40
41.22	22.17	0.02	1.00	0.02	1.36	0.02	227.54	26.85	0.10	–	–	–	–
43.46	22.27	0.02	0.98	0.02	1.36	0.02	230.34	26.95	0.11	–	–	–	–
46.82	22.36	0.02	0.94	0.02	1.35	0.02	233.92	27.05	0.12	–	–	–	–
48.74	22.47	0.02	0.97	0.02	1.35	0.02	–	–	–	–	–	–	–

[a] Units are in mag arcsec^{-1}.

TABLE 4

Kiso Ellipse Fit Luminosity and Color Profiles[a]

a	μ_V	σ	$\mu_V-\mu_R$	σ	a	μ_V	σ	$\mu_V-\mu_R$	σ
0.00	17.15	0.02	0.72	0.03	62.19	22.00	0.02	0.59	0.03
0.52	17.20	0.02	0.72	0.03	68.45	22.10	0.02	0.55	0.03
1.08	17.30	0.02	0.68	0.03	73.16	22.20	0.02	0.55	0.03
1.46	17.40	0.02	0.65	0.03	77.05	22.30	0.02	0.53	0.03
1.76	17.50	0.02	0.64	0.03	79.74	22.40	0.02	0.54	0.03
2.03	17.60	0.02	0.64	0.03	82.77	22.50	0.02	0.55	0.03
2.31	17.70	0.02	0.64	0.03	85.92	22.60	0.02	0.55	0.03
2.59	17.80	0.02	0.64	0.03	88.90	22.70	0.02	0.55	0.03
2.92	17.90	0.02	0.64	0.03	91.14	22.80	0.02	0.56	0.03
3.29	18.00	0.02	0.63	0.03	92.87	22.90	0.02	0.58	0.03
3.70	18.10	0.02	0.62	0.03	94.52	23.00	0.02	0.60	0.03
4.11	18.20	0.02	0.62	0.03	96.58	23.10	0.02	0.60	0.03
4.54	18.30	0.02	0.62	0.03	99.03	23.20	0.02	0.58	0.03
5.03	18.40	0.02	0.63	0.03	101.80	23.30	0.02	0.59	0.03
5.56	18.50	0.02	0.63	0.03	104.78	23.40	0.02	0.60	0.03
6.09	18.60	0.02	0.63	0.03	108.86	23.50	0.02	0.58	0.03
6.63	18.70	0.02	0.64	0.03	112.06	23.60	0.02	0.59	0.03
7.18	18.80	0.02	0.64	0.03	115.05	23.70	0.02	0.59	0.04
7.69	18.90	0.02	0.65	0.03	118.30	23.80	0.03	0.59	0.04
8.24	19.00	0.02	0.66	0.03	122.61	23.90	0.03	0.59	0.04
8.84	19.10	0.02	0.67	0.03	127.93	24.00	0.03	0.59	0.04
9.73	19.20	0.02	0.66	0.03	133.80	24.10	0.03	0.58	0.04
10.62	19.30	0.02	0.66	0.03	139.37	24.20	0.03	0.58	0.04
11.48	19.40	0.02	0.66	0.03	145.03	24.30	0.03	0.58	0.05
12.33	19.50	0.02	0.66	0.03	151.03	24.40	0.04	0.58	0.05
13.21	19.60	0.02	0.66	0.03	156.86	24.50	0.04	0.59	0.05
14.12	19.70	0.02	0.66	0.03	161.86	24.60	0.04	0.59	0.06
15.19	19.80	0.02	0.66	0.03	167.81	24.70	0.05	0.57	0.06
16.39	19.90	0.02	0.65	0.03	175.01	24.80	0.05	0.54	0.07
17.78	20.00	0.02	0.65	0.03	180.74	24.90	0.05	0.56	0.07
19.23	20.10	0.02	0.64	0.03	186.70	25.00	0.06	0.56	0.08
20.62	20.20	0.02	0.65	0.03	192.11	25.10	0.06	0.54	0.09
22.23	20.30	0.02	0.65	0.03	196.34	25.20	0.07	0.55	0.09
24.22	20.40	0.02	0.64	0.03	200.37	25.30	0.07	0.56	0.10
26.47	20.50	0.02	0.64	0.03	204.41	25.40	0.08	0.55	0.11
29.56	20.60	0.02	0.62	0.03	209.27	25.50	0.09	0.55	0.12
31.93	20.70	0.02	0.61	0.03	215.94	25.60	0.10	0.53	0.13
33.55	20.80	0.02	0.62	0.03	222.70	25.70	0.11	0.52	0.14
35.30	20.90	0.02	0.62	0.03	228.87	25.80	0.11	0.50	0.16
37.16	21.00	0.02	0.62	0.03	233.25	25.90	0.13	0.49	0.17
39.05	21.10	0.02	0.62	0.03	238.44	26.00	0.14	0.52	0.19
40.95	21.20	0.02	0.63	0.03	242.35	26.10	0.15	0.56	0.20
43.08	21.30	0.02	0.63	0.03	247.72	26.20	0.16	0.51	0.23
45.28	21.40	0.02	0.63	0.03	251.53	26.30	0.18	0.54	0.24
47.87	21.50	0.02	0.62	0.03	256.14	26.40	0.20	0.51	0.27
50.21	21.60	0.02	0.62	0.03	262.61	26.50	0.22	0.44	0.30
52.69	21.70	0.02	0.62	0.03	263.92	26.60	0.24	0.51	0.32
55.08	21.80	0.02	0.62	0.03	278.04	26.70	0.26	–	–
57.54	21.90	0.02	0.62	0.03	–	–	–	–	–

[a] Units are in mag arcsec^{-1}.

UGC 12591, the fastest known rotating disk system (Giovanelli et al. 1986) and makes this interpretation improbable since such systems are very rare. Also, our analysis of H I velocities in § 8 favors a minimum inclination of 26°.

The isophotal parameters $\log D_{25}$ and $\log R_{25}$ given in Table 1 are significantly different from those given in RC3: 1.64 and 0.025, respectively, versus 1.59 ± 0.02 and 0.08 ± 0.02 in RC3. From our surface photometry, the $\mu_B = 25.00$ mag arcsec^{-2} isophote is much rounder than implied by the RC3 value, which may have been based on visual estimates affected by the high contrast of the outer ring.

4. PROFILE AND FOURIER DECOMPOSITION

4.1. *Two-Component Model*

The ellipse fit profiles in Tables 3 and 4 are nearly equivalent to major axis profiles, and thus are amenable to a standard photometric decomposition. We found that the usual fitting functions, an $r^{1/4}$ spheroid and an exponential disk, work remarkably well for the KPNO profiles of NGC 7217. For the fits, we first removed all points in the profiles associated with the ring features of the galaxy. We then used a nonlinear least-squares routine from Press et al. (1988) to derive the four main parameters of the fitting functions: the effective radii $r_e^{\rm I}$ and $r_e^{\rm II}$ of the spheroid and disk, respectively, and the corresponding effective surface brightnesses $\mu_e^{\rm I}$ and $\mu_e^{\rm II}$. The results of the fits are compiled in Table 5 and displayed in Figures 9*a*–9*d*. For all three filters, the model indicates that the spheroid dominates over most of the area beyond the outer ring. To compute the spheroid-to-disk luminosity ratio, we need an estimate of the apparent disk axis ratio. A first approximation is provided by the minimum observed isophotal axis ratio, 0.83. Using equations (2) and (3) of Simien & de Vaucouleurs (1986), we find that the spheroid contributes 70% and the disk (exponential part plus the outer ring) contributes 30% of the total blue luminosity. Thus, the spheroid-to-disk ratio is about 2.3 and the fractional contribution of the spheroid in magnitudes is $\Delta m_{\rm I}(B) = -2.5 \log k_{\rm I} = 0.39$ mag. This latter quantity is smaller than the typical bulge-to-disk ratio for Sab galaxies (Simien & de Vaucouleurs 1986), meaning the spheroid is a more significant contribution to the total luminosity in NGC 7217.

On the other hand, the dominance of the rounder component suggests that the true disk axis ratio could be less than the minimum observed ratio. To evaluate this, we subtracted the blue light spheroid model from the *B*-band image and fitted ellipses to the residual intensities, presumed to be entirely attributable to the disk. The results suggest that the true disk flattening could be as low as 0.80. In this circumstance we obtain $k_{\rm I}(B) = 0.702$, $k_{\rm II}(B) = 0.253$, $k_{\rm III}(B) = 0.045$, a total model magnitude of 10.93, and a spheroid-to-total disk ratio of 2.4.

The profiles derived from the Kiso images could not be fitted as well with our adopted fitting functions. To highlight the differences, we show in Figure 9*d* how the *V*-band model derived from the KPNO image compares with the Kiso *V*-band image. The model represents the profile well for $a < 130''$, as expected from Figure 8*a*, but at larger radii there is more light in the Kiso profile. It is essential to obtain independent images with another wide field CCD to resolve this discrepancy, which could be caused by the very bright stars in the field. Because of this disagreement our decompositions are only tentative, but this does not compromise our basic result that the outer isophotes of the galaxy are much rounder than the inner ones. The KPNO and Kiso images are in very good agreement on the shapes of the isophotes in the outer regions.

TABLE 5

DECOMPOSITION PARAMETERS FOR NGC 7217[a]

Parameter	*B*	*V*	*I*
$\mu_e^{\rm I}$ (mag arcsec^{-2})	23.30 ± 0.07	22.16 ± 0.08	20.86 ± 0.08
$r_e^{\rm I}$	$53''.3 \pm 2''.4$	$50''.0 \pm 2''.4$	$52''.0 \pm 2''.5$
$\mu_e^{\rm II}$ (mag arcsec^{-2})	23.52 ± 0.14	22.50 ± 0.16	21.14 ± 0.16
$r_r^{\rm II}$	$53''.5 \pm 3''.1$	$49''.9 \pm 3''.4$	$49''.1 \pm 3''.3$
k_I	0.696	0.731	0.752
$k_{\rm II}$	0.260	0.244	0.236
$k_{\rm R}$	0.044	0.025	0.012
m_T	10.92	9.99	8.63

NOTES.—μ_e and r_e are the effective surface brightness and effective radius, respectively, of a fitted component (I: spheroid, II: disk); k is the fractional contribution of a given component to the total luminosity, where the values assume a spheroid axis ratio of 0.96 and a disk axis ratio of 0.83 ($k_{\rm R}$ refers to the outer ring); m_T is the total magnitude of the combined model.

[a] Based on KPNO images only.

4.2. *Checks on the Model*

The two-component model of the light distribution described in the previous section represents the major axis profile only. It does not necessarily follow that the model is unique, nor does the good fit imply that the two-dimensional light distribution is represented by it. One way of further testing this model is to predict isophote shapes. Using the parameters for the *B* band in Table 5, and adopting fixed disk and spheroid axis ratios and position angles, we can combine the models, fit ellipses to the combined model isophotes, and compare the results with ellipse fits made to the actual galaxy isophotes. The results for $q_d = 0.80$, $q_{\rm sph} = 0.96$, and $\theta_0 = 91°$ are shown by the solid curve in the lower panel of Figure 6. The agreement with the observed *B*-band axis ratios (*filled circles*) is not good, especially in the radius range $90'' < a < 140''$. Thus, the simple two-component model provides a good representation of the major axis profile, but does not represent the two-dimensional light distribution in detail. Details in Figure 6 could be caused by a combination of factors, such as spiral structure in the rings and variations in internal extinction.

We have also tried forcing the disk to be dominant in the intermediate regions, to see if a more reasonable bulge model might follow. For this purpose, we forced the disk scale length to be consistent with the slope of the luminosity profile under the outer ring and then varied the central surface brightness. Figure 9*e* shows the net *B*-band surface brightness after subtraction of the disk model with the maximum allowed central surface brightness for the chosen scale length and also after subtraction of the disk model in Table 5. The results show that the surface brightnesses in the inner bulge region are not greatly affected by the increased disk light compared to the adopted model, but the bulge would necessarily truncate in the intermediate disk region. It is of course entirely possible that another spheroid model other than the $r^{1/4}$ law could be applicable to this galaxy. However, we feel the combined $r^{1/4}$ bulge, exponential disk model is the simplest, most reasonable two-component model we can derive.

4.3. *Three-Component Model*

The spheroidal component in NGC 7217 appears to be much larger in extent than is typical for galaxies of its type.

Bulges are normally thought of as highly concentrated, rapidly rotating components of high metallicity, while stellar halos are normally thought of as slowly rotating components of low metallicity (see Gilmore, King, & van der Kruit 1989, p. 3). We have considered, in a very simple manner only, a three-component model whereby the stellar halo is a separate component from the bulge and disk. We investigated the feasibility of this by considering results for the stellar halo of the Milky Way. This halo has a power-law density distribution with a slope of -3.5, based on globular clusters (Zinn 1985). If the stellar halo of NGC 7217 follows a similar power law, then a plot of surface brightness versus log (radius) should be linear in the region dominated by the halo (for constant mass-to-light ratio). According to Figure 6, this region could cover radii $a > 140''$ because here the axis ratio is roughly constant at $\langle q \rangle = 0.96$. Figure 9*f* shows a plot of μ_B versus log a over the whole radius range available. The solid line is the fit for the assumed halo-dominated region. It is clear that the line cannot be extrapolated into the inner regions, and therefore a three-component model with a power-law stellar halo is unfeasible unless the halo truncates in the inner regions, or the effects of internal extinction in the disk are serious (see § 10.3). Use of the profiles obtained in the other filters would lead to a similar conclusion.

4.4. *Fourier Analysis*

Using our decomposition parameters we have approximated the deprojected appearance of NGC 7217 in *B* and *I* as follows. First, we subtracted the spheroid models in Table 5 from the intensity arrays using the axis ratio and position angle in Table 1. Second, we used the IRAF program IMLINTRAN to deproject the residual light, assuming all of it to be associated with a very thin disk. For this purpose, we assumed a disk axis ratio of 0.83, the minimum observed ratio in Figure 6. This is mostly a compromise between the spheroid-corrected disk axis ratio of 0.8, and the ratio of 0.87–0.90 implied by the H I velocity field analysis. Finally, we added back the spheroid light after making a small correction for its tilt. The resulting deprojected images are shown in the upper panels of Figure 10 (Plate 30). IMLINTRAN was used in flux-conserving mode so that we could derive reliable Fourier intensity amplitudes. These amplitudes were obtained from circular averages of the intensities as described by Buta (1986b). The relative amplitudes and phases of the $m = 2$ term are plotted versus normalized radius a/a_{25} (where $a_{25} = 131''.9$ is the radius of the $\mu_B = 25.0$ mag arcsec^{-2} isophote; $D_{25} = 2a_{25}$) in Figure 11 for both *B* and *I*. In both filters, there is almost no significant $m = 2$ amplitude over the whole disk-dominated region. If the adopted orienta-

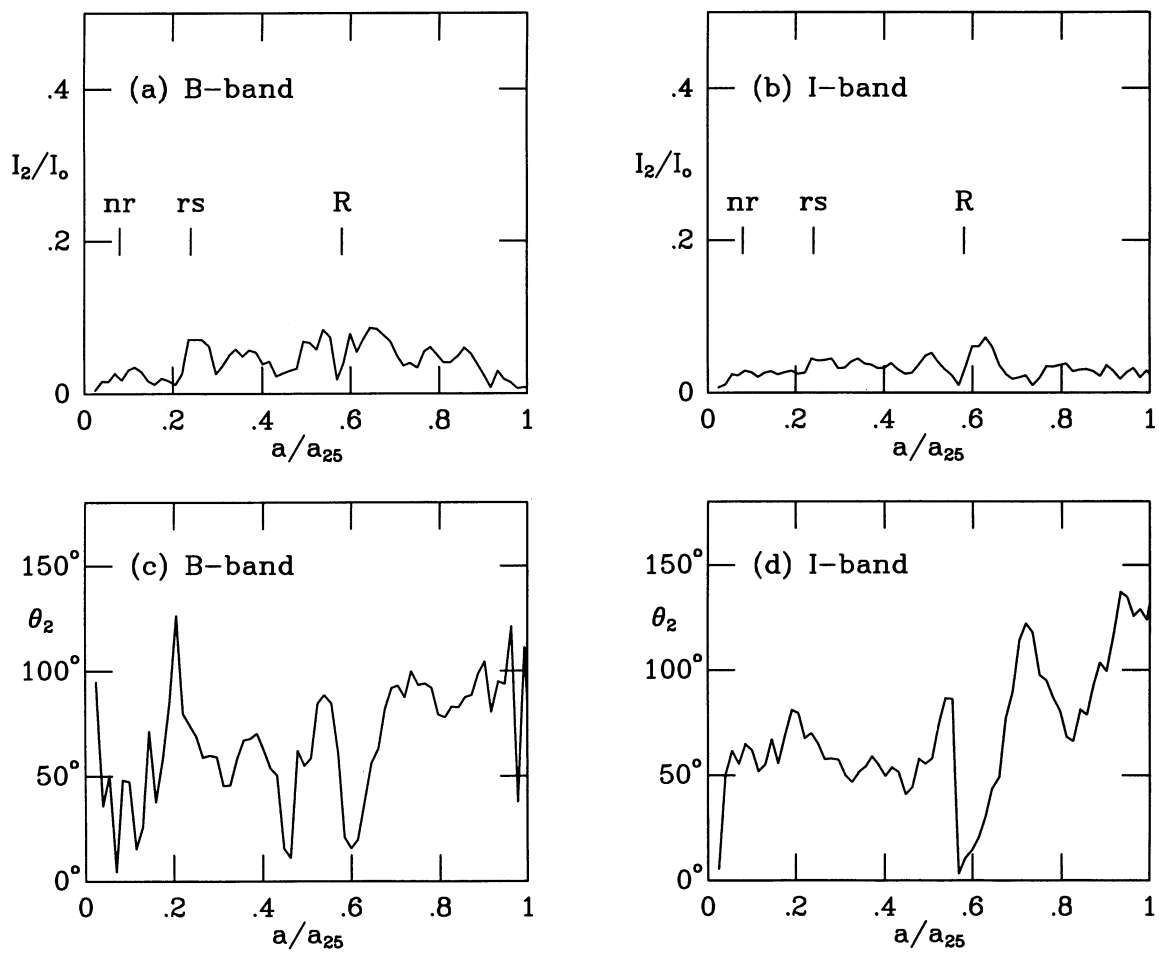

FIG. 11.—Relative Fourier amplitudes and phases for the $m = 2$ component of the luminosity distribution of NGC 7217 as a function of normalized radius, for the *B* and *I* passbands. For the plot, the isophotal radius $a_{25} = 131''.9$.

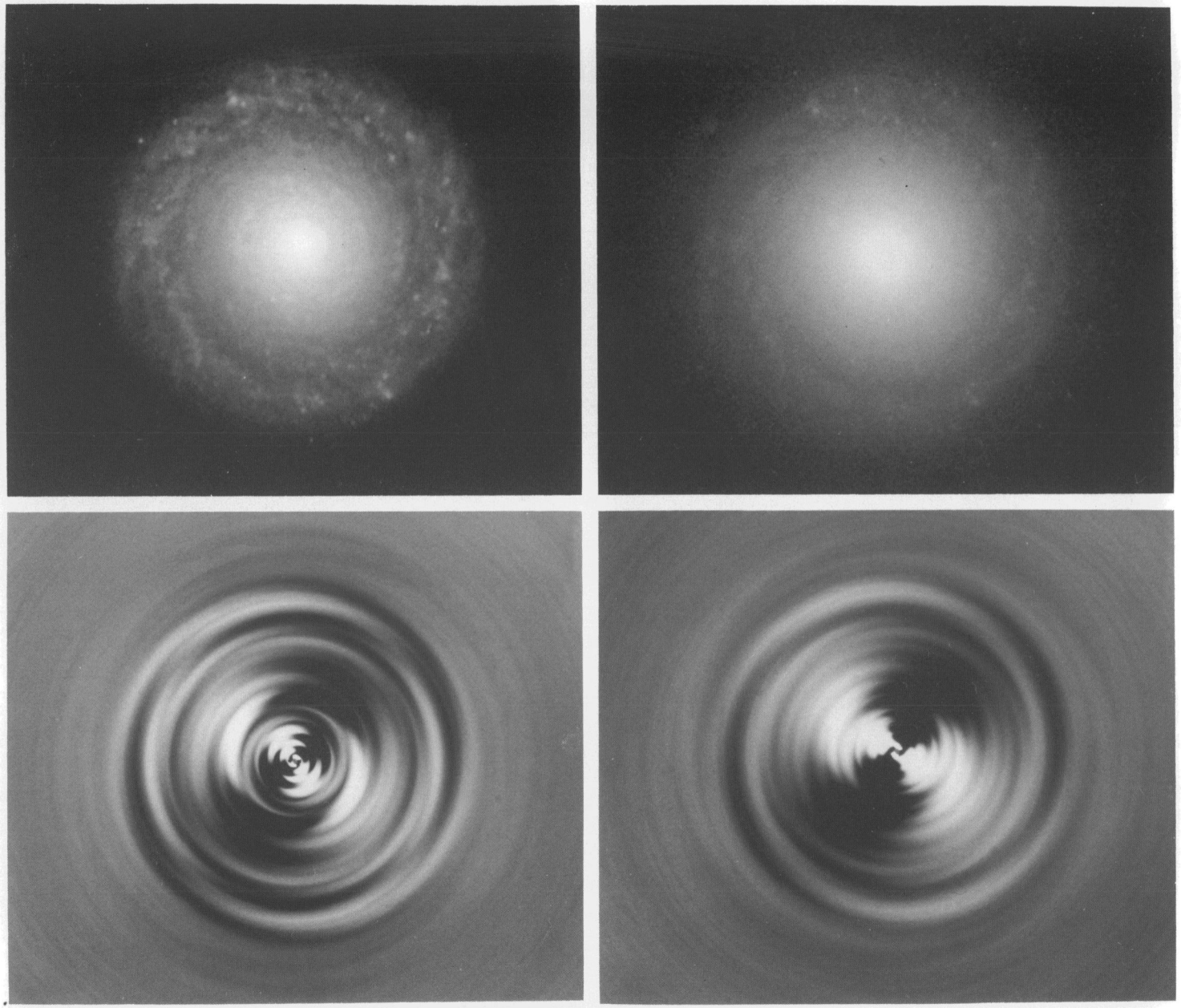

FIG. 10.—*Upper left*, deprojected *B*-band image of NGC 7217; *upper right*, deprojected *I*-band image; *lower left*, image of the $m = 2$ Fourier component in the *B* band, based on Figs. 11*a* and 11*c*; *lower right*, image of the $m = 2$ Fourier component in the *I* band, based on Figs. 11*b* and 11*d*. Note the clear two-armed spiral in the outer ring region and the barlike distortion in the inner regions.

TABLE 6

OUTER RING MAGNITUDE AND COLORS[a]

Parameter	B	$B-V$	$V-R$	$V-I$	$(B-V)_0$	$(V-R)_0$	$(V-I)_0$
Total R.....	12.63	0.81	0.57	1.27	0.68	0.51	1.12
Background of R.....	12.89	0.92	0.60	1.35	0.79	0.54	1.20
Net R.....	14.30	0.30	0.34	0.60	0.17	0.28	0.46

[a] B, $B-V$, and $V-I$ are based on KPNO images; $V-R$ is based on Kiso images.

tion parameters are correct, then NGC 7217 is a very axisymmetric galaxy. Nevertheless, Figure 11*d* shows a very well-defined phase pattern: the position angle of the $m = 2$ I-band component is nearly constant at about 60° for $0.05 \leq a/a_{25} \leq 0.4$, while in the vicinity of the outer ring ($0.45 \leq a/a_{25} \leq 0.75$), the phase changes smoothly with radius. The B-band phases seem less systematic by comparison. To illustrate what these characteristics mean, the lower panels of Figure 10 illustrate reconstructed $m = 2$ images in B and I, respectively. The B-band $m = 2$ image shows little evidence for clear, continuous spiral structure, but the I-band $m = 2$ image definitely shows a two-armed spiral pattern in the region of the outer ring and a weak barlike distortion in a position angle of about 60°. Thus, NGC 7217 does indeed have measurable nonaxisymmetry in its stellar distribution.

Note that the Fourier amplitudes are very sensitive to the adopted orientation parameters, and that virtually any other choice of parameters will increase the significance of the nonaxisymmetric terms. This is because a disk axis ratio of 0.83 and a disk position angle of 91° circularizes the outer ring, a feature which is more likely to be slightly noncircular. This is discussed further in § 9.

5. THE OUTER RING

The outer ring of NGC 7217 differs from other examples such as NGC 1433 (Buta 1986b), NGC 1291 (de Vaucouleurs 1975), and NGC 7020 (Buta 1990) in that the background can be reliably interpolated under the ring. To determine the net fluxes and colors of the ring, we computed azimuthally averaged profiles for each filter using elliptical annuli with fixed axis ratio 0.83 and major axis position angle 91°. We then fitted a low-order polynomial to surrounding intensities over a range of radii on either side of the ring. The background was subtracted and the net flux integrated within the ring region. Table 6 gives the net ring magnitude and colors, and in addition gives the integrals for the background alone and the total background plus ring. The last three columns of Table 6 give the color corrected for inclination, galactic extinction, and redshift using RC3 procedures. The net colors are very blue and indicate a very stellar young population. The background colors are very much redder and indicate a much older population.

To interpret the meaning of the net ring colors, we show in Figure 12 color-color plots using large samples of normal galaxies for comparison. Corrected total $B-V$ colors are from RC3, but the corrected total $V-R$ and $V-I$ colors are from a related study by Buta & Williams (1995; see also Buta & Crocker 1992). The colors of the outer ring of NGC 7217 fall close to the mean relations for normal galaxies and are similar to those for late-type spirals and irregulars. Hence, it is possible that the feature has been a zone in the disk which has had a nearly uniform star-formation rate for much of the lifetime of the galaxy. As we show in the next sections, the outer ring is the locus of most of the neutral gas in NGC 7217.

6. 21 CENTIMETER H I LINE RADIO SYNTHESIS OBSERVATIONS

Observations of NGC 7217 in the 21 cm line of neutral hydrogen were obtained with the Westerbork Synthesis Radio

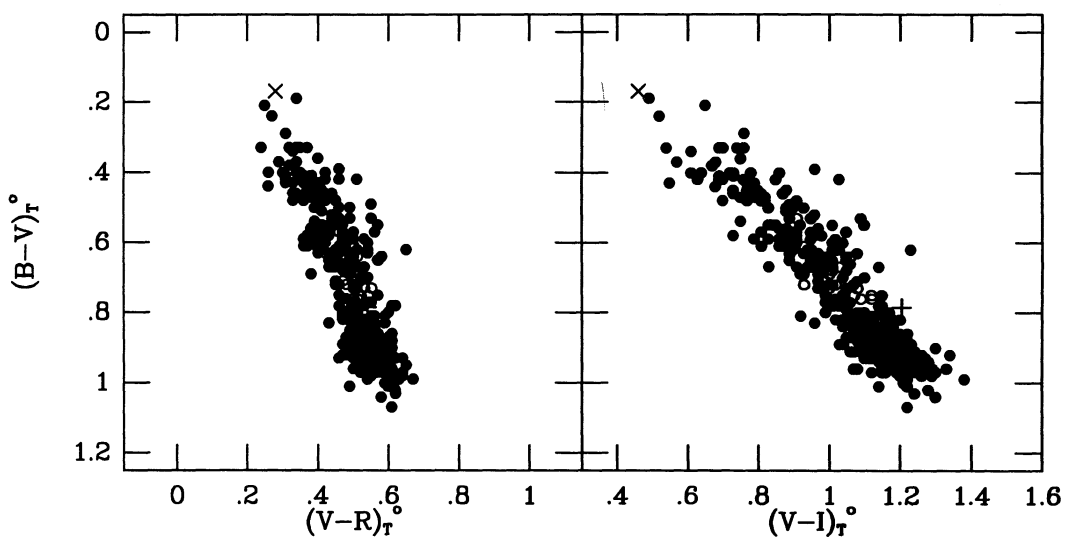

FIG. 12.—Two-color plot of the net colors of the outer ring (*large cross*) and integrated colors (*large plus*) of NGC 7217. For comparison, the diagram shows the colors of a large sample of normal galaxies over all types from Buta & Williams (1995; *filled circles*) and for a smaller sample of ringed galaxies from Buta & Crocker (1992; *open circles*).

TABLE 7

PARAMETERS OF H I LINE OBSERVATIONS

Parameter	Value
Observation date	1991 April 27
Integration time (hr)	12
Baselines[a] (m)	36(72)2712
Field center (α, 1950)	$22^h05^m37^s.8$
Field center (δ, 1950)	+31°06′48″
Primary beam	36′
Map size ($\alpha \times \delta$)	21′ × 40′
Synthesized beam ($\alpha \times \delta$)	12″.6 × 24″.4
Central heliocentric velocity (km s^{-1})	946
Effective bandwidth (km s^{-1})	945
Channel separation (km s^{-1})	16.6
Velocity resolution (km s^{-1})	33
rms noise (mJy beam^{-1})	0.98

[a] Shortest (increment) longest spacing.

Telescope (WSRT) in 1991. A summary of observational and instrumental parameters is given in Table 7. For references to the instrument and standard WSRT data handling procedures see, e.g., Mulder & van Driel (1993). The data were calibrated using standard continuum sources. Data were obtained simultaneously in 64 frequency channels over a total effective bandwidth of 945 km s^{-1}. A Hanning velocity tapering was applied, giving a velocity resolution of 33 km s^{-1}, i.e., twice the channel separation. The data were edited to eliminate interferometers with bad response and interference signal and then Fourier transformed, giving maps of the brightness distribution in each velocity channel. The subsequent data reduction was carried out with the interactive GIPSY system (Allen, Ekers, & Terlouw 1985; van der Hulst et al. 1992).

6.1. *Radio Continuum Emission*

Twenty-three velocity channels at the extremes of the bandwidth were found to be free of line radiation, and these channel maps were averaged into a map of the continuum radiation in the field. We CLEANed (Högbom 1974) this full-resolution (HPBW = 13″ × 25″, $\Delta\alpha \times \Delta\delta$) map, and found a central 11 mJy point source only, i.e., no extended disk emission.

VLA 20 cm observations with a resolution of about 45″ (Condon 1987; Gioia & Fabbiano 1987) show a central point source with a flux density of about 16 mJy, about 50% higher than our value. High-resolution (1″.3 HPBW) 20 cm VLA observations (Hummel et al. 1987) show a 5 mJy nuclear source with an intrinsic size of about 0″.6, slightly elongated along p.a. 165°, i.e., roughly perpendicular to the elongation of the outer regions. The presence of such a relatively strong subarcsecond source in the nucleus of NGC 7217, which supports the optical evidence for mild nuclear activity, is much more common in early-type and ringed spirals, such as NGC 7217, than in other morphological types (Braine 1992).

The 21 cm radio power of the galaxy derived from the Westerbork data is log ($P_{1.4}$/W Hz^{-1}) = 20.5, a rather high value for a central source in a spiral galaxy (see Hummel 1981); only about 15% of spirals have a higher radio power.

6.2. *Channel Maps and Global* H I *Content*

An average of the continuum channel maps was subtracted from all of the channel maps, revealing the net H I emission (see Fig. 13). The maps were smoothed to a 25″ × 25″ HPBW resolution, after subtraction of the continuum, in order to better show the relatively faint line emission in the galaxy. A global H I profile (Fig. 14) was derived by integrating each channel map over an area surrounding the H I line emission and correcting for the attenuation of the primary beam. The basic parameters derived from the profile are listed in Table 8. We derive a total H I mass of $M_{\rm H\,I} = 0.58 \times 10^9\ M_\odot$, implying $M_{\rm H\,I}/L_B^0 = 0.024\ M_\odot/L_{\odot,B}$, a very low ratio compared to the value of about 0.13 found for normal Sab-type galaxies (Buta et al. 1994), indicating that NGC 7217 is quite H I gas poor for its morphological type. Our global profile agrees well with the single-dish profiles published by Balkowski & Chamaraux (1983), Bottinelli, Gouguenheim, & Paturel (1980a), Davies & Seaquist (1983), Giovanelli & Haynes (1985), Hewitt, Haynes, & Giovanelli (1983), and Peterson et al. (1978); see also the compilations by Huchtmeier & Richter (1989) and Paturel et al. (1990).

6.3. H I *Distribution and Velocity Field*

Figure 15 shows a map of the H I column density distribution, smoothed with a HPBW resolution of 25″ × 25″ in order to better reveal faint line emission. The map was made using the so-called conditional transfer method (see, e.g., Bosma 1981), in which only those pixels in the 25″ × 25″ resolution channel maps are added where the brightness temperature exceeds the 2 σ level in the corresponding channel maps smoothed to a 60″ × 60″ resolution. The map shows that the H I is distributed in a ring having a ridge-line diameter of 1′.3 and an axis ratio of 0.82. This ring almost precisely coincides with the optical, blue outer ring (see Table 2 parameters). The center of symmetry of the H I ring, however, lies about 10″ south of the optical center, while the blue light ring seems well centered on the nucleus.

The azimuthally averaged H I surface density (corrected to face-on), $\sigma_{\rm H\,I}$, as a function of radius (Fig. 16) was derived from the full-resolution H I column density distribution (not shown here). For the center position we used the optical value listed in Table 1, and for the major axis position angle and the axial ratio we used 275° and 0.87, respectively, based on the kinematic analysis in the next section. The depth of the central depression in the H I distribution is comparable to that found in other outer-ringed galaxies of type Sa to Sb (van Driel & van Woerden 1994), as the central $\sigma_{\rm H\,I}$ is about 1 $M_\odot$ pc^{-2}. The maximum of $\sigma_{\rm H\,I} \sim 4\ M_\odot$ pc^{-2} is reached at about 4.2 kpc radius in the H I ring. The H I radius at a level of $\sigma_{\rm H\,I} = 1.0\ M_\odot$ pc^{-2} is 7 kpc ($= 0.8 a_{25}$).

The H I distribution of NGC 7217, with its central depression and concentration of gas in the outer optical ring, resembles that of other spirals with optical outer rings, though its maximum $\sigma_{\rm H\,I}$ is (of course) higher then the values found in galaxies of type RSB0/a or RSBa (see, e.g., van Driel & Buta 1991; Mulder & van Driel 1993; van Driel & van Woerden 1991, 1994).

The H I velocity field (Fig. 17) was derived by determining an intensity-weighted mean velocity $\langle V \rangle = \Sigma T_b(V) \times V / \Sigma T_b(V)$ at each pixel, summing over the velocities in which H I emission was found in channel maps with a resolution of 25″ × 25″, which were masked with 60″ × 60″ resolution reference channel maps in the same way as the full-resolution maps (see above). The velocity field shows the typical pattern of a galaxy in differential rotation.

6.4. *Rotational Velocities*

A position-velocity diagram along the H I major axis of NGC 7217 (p.a. 265°) is shown in Figure 18; it clearly shows

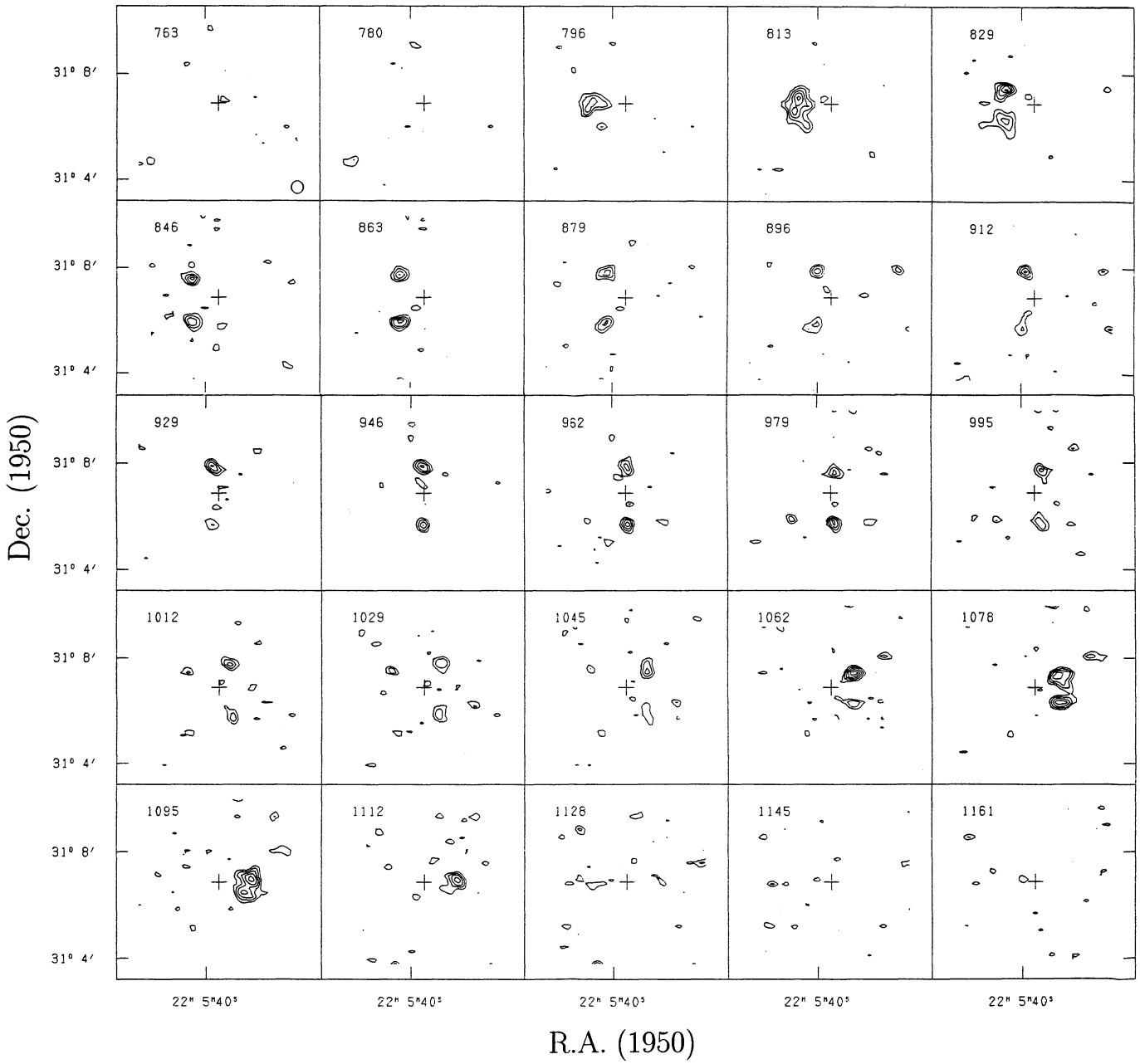

FIG. 13.—H I line channel maps smoothed to a HPBW resolution of 25″ × 25″. Contour levels are −1.8, −1.2, and 1.2 to 4.1 in steps of 0.56 mJy per beam. Negative contours are dashed, and the rms noise is 0.56 mJy per beam. The central heliocentric velocity is shown in each channel map. The cross indicates the optical center of the galaxy.

the limited range in radius at which H I emission was detected. We also derived a H I rotation curve for the galaxy (see Fig. 19 and Table 9), by making least-squares fits to the observed velocity field around circular rings in the plane of the galaxy (see Begeman 1989 and Warner, Wright, & Baldwin 1973). Rotational velocities were determined separately for the approaching and receding halves of the galaxy, as well as for the entire disk. As the center position and systemic velocity (see Table 1) were the only fixed parameters in the fits, we also determined the kinematical inclination and major axis position angle as functions of radius. Points within a sector of ±30° of the minor axis were excluded from the fits. Due to the narrow, ring-shaped H I distribution, rotational velocities could only be determined from about 3.5–7 kpc radius, a range which is barely twice the linear resolution of 2 kpc (see Fig. 15). The errors shown were determined from the differences between the rotation curves of both halves, as well as from the fit per ring. At 4.2 kpc radius the model fits would not yield a satisfactory solution for the approaching (eastern) half of the disk; therefore, a colon is appended to the parameters derived for this radius. The major axis position angle of the fits made to the entire disk and the receding half is rather constant at 285°, while that of the approaching half is consistently some 20° lower.

These values should be compared with the adopted photometric major axis position angle of 91° (271°) and the adopted

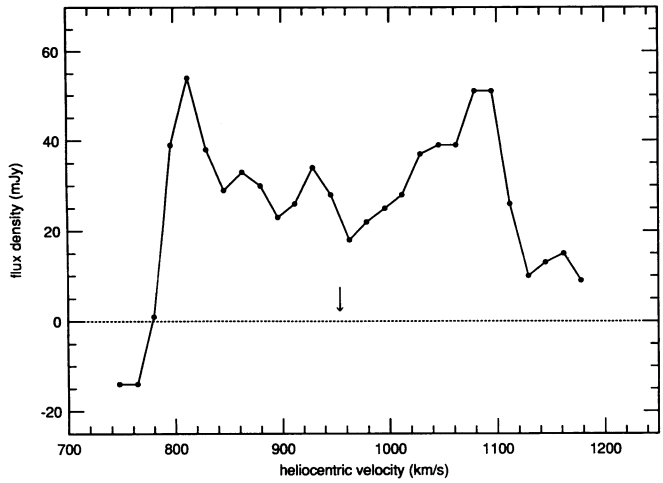

FIG. 14.—Global H I profile, derived as explained in the text. The arrow indicates the mean velocity.

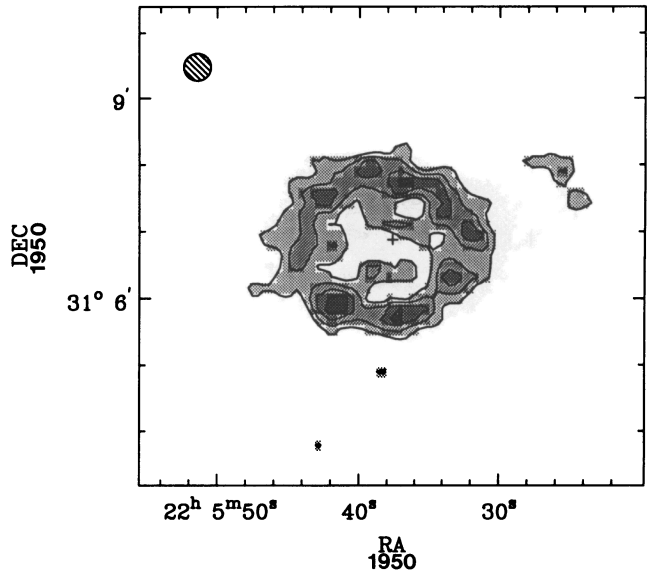

FIG. 15.—Map of the H I column density distribution in NGC 7217 with a HPBW resolution of 25″ × 25″. Contour levels are 2.9, 5.1, 7.3, and 9.4 × 10^{20} cm^{-2}. The beam size is indicated by the hatched circle in the upper left corner. The cross indicates the center of the galaxy.

inclination of 35°. The H I major axis position angle and the derived kinematic major axis position angle bracket the photometric one and are not significantly different from it. The lower inclination given by the fits to the H I data is a more serious disagreement, especially if the true disk axis ratio is more like 0.8 (implying $i = 38°$). However, the algorithm of Begeman (1989) does not yield accurate inclinations when the inclination is less than about 40°.

The mean rotational velocity is about 265 km s^{-1}. Within the last point at $R = 6.9$ kpc ($=0.74a_{25}$ or ≈ 3 optical disk scale lengths according to the decomposition parameters in Table 5), we estimate a total mass of $M_T \sim 0.9 \times 10^{11}\ M_\odot$, or $M_T/L_B^0 \sim 4\ M_\odot/L_{\odot,B}$, assuming a spherical mass distribution. This is a somewhat low but not unexceptional global mass-to-light ratio for a spiral within the standard isophotal radius (see, e.g., van Driel & van Woerden 1991).

Kent (1986) fitted disk/bulge/halo mass models to the optical rotation curve of Rubin et al. (1985) and concluded (like Kalnajs 1983) that mass models without a dark halo yielded the best fit to the data. Our new H I data would not have changed his conclusion. Forbes (1992) found that NGC 7217 is one of the rare galaxies in which the total mass-to-light ratio is rather constant with radius.

TABLE 8

DERIVED GLOBAL RADIO PROPERTIES

Parameter	Value	Reference
$\int S\,dV$ (Jy km s^{-1})	11.8	*
$\int S\,dV$ (Jy km s^{-1})	11.7	D
$M_{\rm H\,I}$ ($M_\odot$)	0.58×10^9	*
$M_{\rm H\,I}/L_B^0$ ($M_\odot/L_{B\odot}$)	0.024	*
Heliocentric radial velocity (km s^{-1})	954	*
Heliocentric radial velocity (km s^{-1})	950	D
Profile width W_{50} (km s^{-1})	320	*
Profile width W_{20} (km s^{-1})	341	*
Profile width W_{20} (km s^{-1})	353	D
21 cm continuum flux density (mJy)	10.6	*
Radio power log ($P_{1.4}$/W Hz^{-1})	20.5	*

REFERENCES.—(D) Davies & Seaquist 1983; (*) this paper.

7. CO LINE OBSERVATIONS

NGC 7217 was mapped partially in the CO(1–0) and CO(2–1) lines with the 30 m telescope of the Institut de Radioastronomie Millimétrique (IRAM) in Pico Valeta, Spain. The beamsizes are about 23″ and 12″ in the (1–0) and (2–1) lines, respectively. The observing procedure was described by Braine et al. (1993). All data are presented using the main beam temperature scale ($T_{\rm mb}$), appropriate for sources only slightly greater than the beam size. CO line spectra were obtained for a total of 13 pointing positions in the galaxy, nine on a 3 × 3 square grid with 7″ spacing centered on the nucleus, one 14″ to the west, and three points with 20″ spacing north of the nucleus. The individual CO(1–0) and CO(2–1) line spectra are shown in Figures 20*a* and 20*b*. Figure 21 shows a direct sum (equal weighting) of the nine central spectra in each line; total

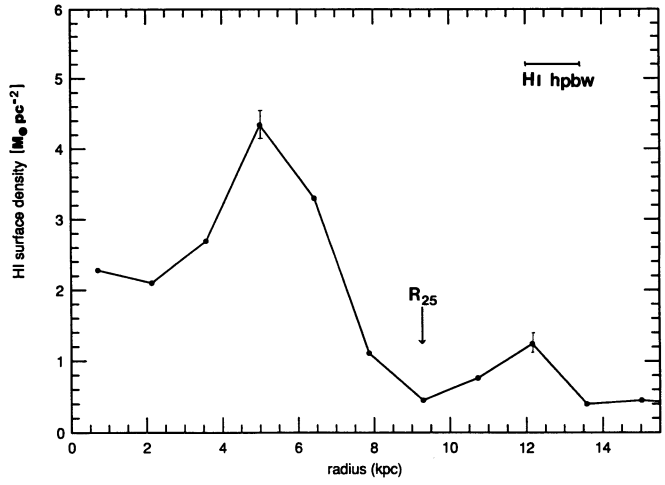

FIG. 16.—Radial distribution of the azimuthally averaged H I surface density, $\sigma_{\rm H\,I}$ (corrected to face-on) in NGC 7217, derived as explained in the text. The mean resolution is indicated as well.

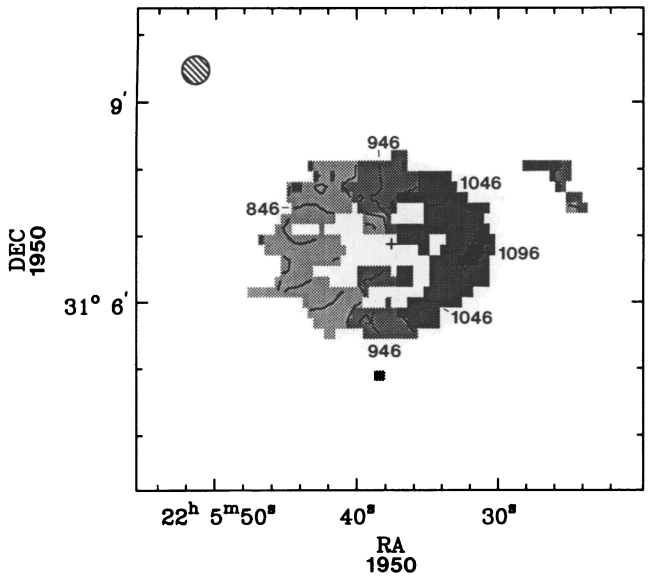

FIG. 17.—H I velocity field with a resolution of 25″ × 25″ (*hatched circle*), made as explained in the text. Isovelocity contours are 846 to 1096 in steps of 50 km s^{-1}. The cross indicates the center of the galaxy.

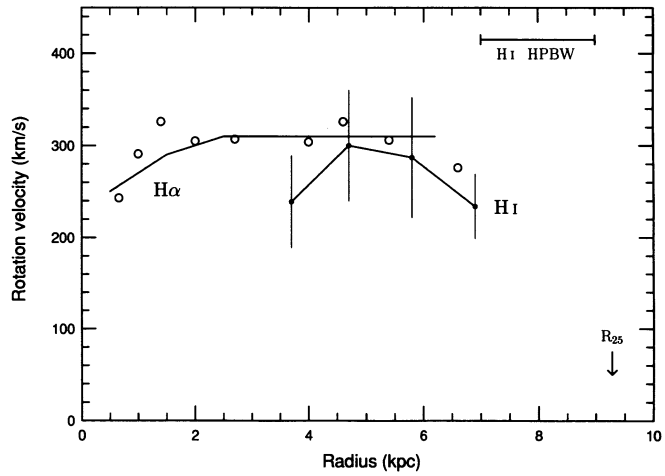

FIG. 19.—H I rotation curve (*filled circles with error bars*) of NGC 7217, made as explained in the text, together with the Hα rotational velocities (*open circles*) from Peterson et al. (1978), Rubin et al. (1985), and new Okayama data (see § 8) corrected for the mean inclination (30°) derived from the H I data. The error bars for the H I data (see Table 4) are derived as described in the text. Also indicated is the 25″ resolution of the H I data.

integrated intensities are about 8 ± 1 K km s^{-1} in both lines. Braine et al. (1993) show the central CO(1–0) and CO(2–1) spectra convolved to roughly 26″ resolution. Total line intensities, $\int T_{mb}\,dV$, of 10 and 9 K km s^{-1} were derived for the CO(1–0) and (2–1) lines, respectively, yielding a CO(2–1)/CO(1–0) line intensity ratio of 0.9, which is the average value for the central regions of galaxies (Braine & Combes 1992). From the CO(1–0) data we derive a total H_2 mass of 2 × 10^8 $M_\odot$ in the region sampled by the nine central spectra (roughly a square 36″ on each side) using a CO–H_2 conversion factor of 2.3 × 10^{20} cm^{-2}/(K km s^{-1}) (Strong et al. 1988).

Global H_2 masses of 8.3, 6.4, and 4.5 × 10^8 $M_\odot$ (corrected for the distance and difference in the CO–H_2 conversion factor) were estimated for NGC 7217 by Young et al. (1989) and Verter (1987)—before and after extrapolation, respectively, from CO (1–0) line observations with the larger beams of the 14 m FCRAO and 7 m Bell Laboratories telescopes. These total H_2 masses are a factor of 2 to 4 higher than the mass

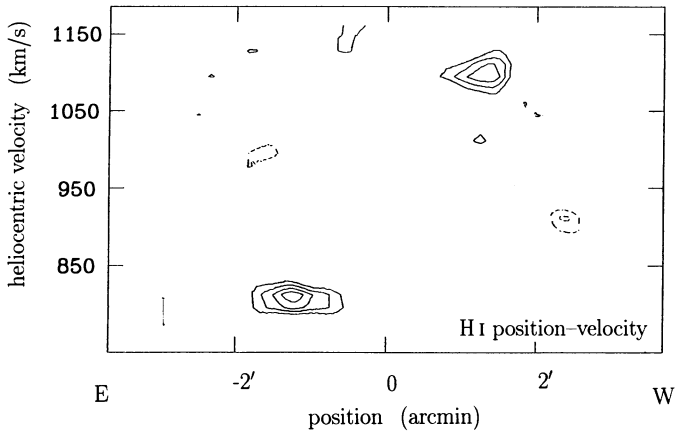

FIG. 18.—Position-velocity plot along the H I kinematical major axis of NGC 7217 (p.a. 265°). Contour levels are −1.8, −1.2, and 1.2 to 2.9 in steps of 0.56 mJy per beam. Negative contours are dashed, and the rms noise is 0.56 mJy per beam. The resolution (25″ × 33 km s^{-1}) is indicated in the upper left corner.

estimated for the inner region from the IRAM spectra, supporting the idea that most of the neutral gas and star formation is indeed in the outer ring. Taking the intermediate value for the H_2 mass, up to about 4.4 × 10^8 $M_\odot$ of H_2 could be in the outer ring, making it marginally dominated by the H I.

The off-center CO spectra show tentative detections in both lines but the S/N is poor and the velocities of the line centers are not always in agreement. In the inner part of the outermost ring, the area covered by the CO observations, the H_2 and H I column densities appear about equal (e.g., slightly below 10^{21} cm^{-2}), making the H_2 mass a factor of 2 greater in this part of the ring. We believe that these tentative detections are real because the velocities are in reasonable accord with the H I velocities at these points. The higher CO(1–0) velocities observed may be due to a slight misalignment of the 3 mm receiver; this would also explain the different shapes of the central profiles (Fig. 21). These data, therefore, support a H_2 mass of at least the Verter value, 6.4 × 10^8 $M_\odot$.

These values of Young et al. and Verter indicate that the total H_2 mass of NGC 7217 is comparable to or somewhat greater than its total H I mass (0.58 × 10^9 $M_\odot$), a high but not extreme H I-to-H_2 mass ratio for its morphological type (Young & Knezek 1989). The total H_2 mass estimated by Verter (1987) indicates a global "star-formation efficiency" of L_{FIR}/M_{H_2} = 7.4 in solar units, a rather normal value for a spiral galaxy, whereas for classical starburst galaxies it is several times higher.

We can use the radio continuum emission to try to estimate the star-formation rate in the different parts of the galaxy. Using the tightness of the correlation between FIR and radio continuum emission for spiral galaxies, Braine (1992) derived a relationship between the 20 cm (or 21 cm) power and massive star-formation rate. If the total flux is 16 mJy from the lowest resolution observations (Condon 1987), and assuming that the 11 mJy flux detected by us comes from the inner regions and that 5 mJy comes from a nuclear point source (Hummel et al. 1987), then the two star-forming rings in NGC 7217 could generate about 5 mJy each. In this case, the massive star-formation rate should be slightly below 0.1 $M_\odot$ yr^{-1} in each ring or about 0.2 $M_\odot$ yr^{-1} per ring for a Miller-Scalo IMF (Scoville & Young 1983).

TABLE 9

PARAMETERS FOR H I ROTATION CURVE

Radius	Radius (kpc)	v_{rot} (km s^{-1})	Error (km s^{-1})	Inclination	Error	Position Angle	Error
52″.5.....	3.7	239:	50	30°:	...	285°:	...
67.5.....	4.7	300	60	26	3°	274	10°
82.5.....	5.8	287	65	28	4	284	15
97.5.....	6.9	234	35	30	10	285	20

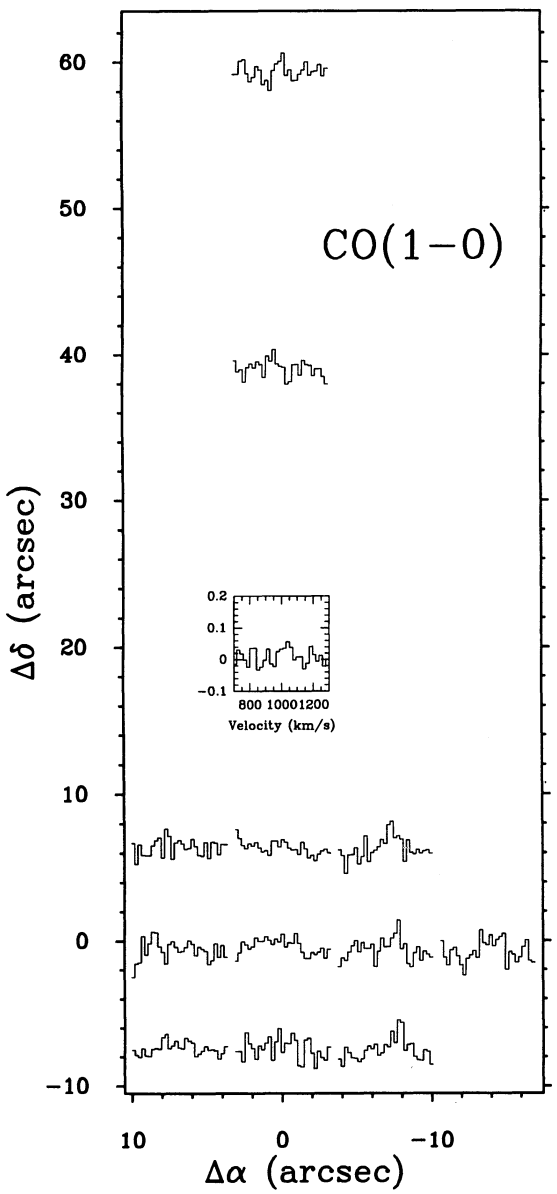

FIG. 20*a*

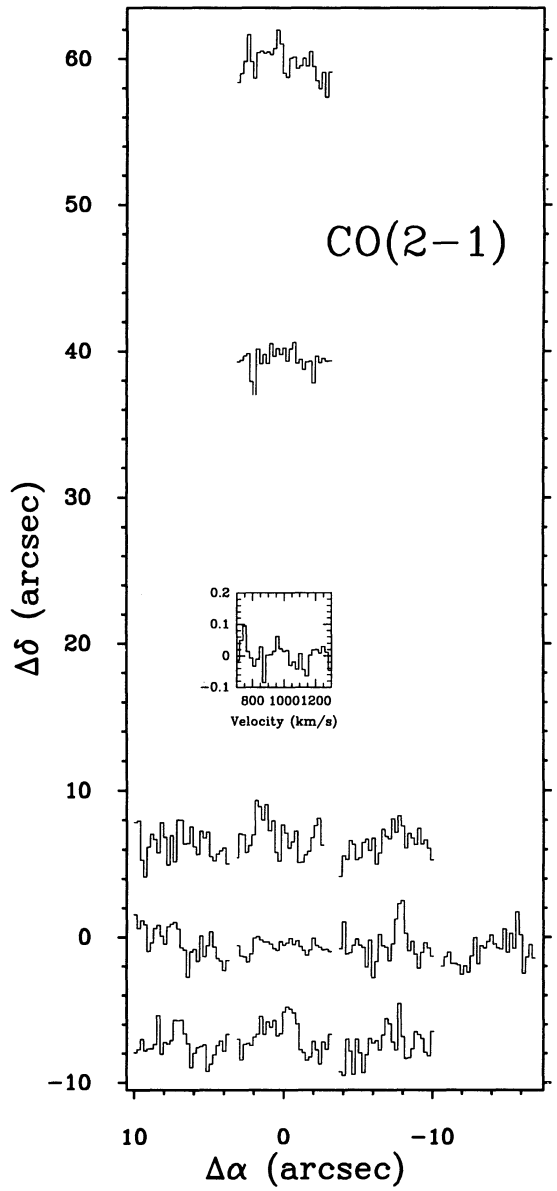

FIG. 20*b*

FIG. 20.—CO line spectra of NGC 7217. (*a*) Mosaic of 13 CO(1–0) line spectra. For each spectrum the range in heliocentric velocity (*horizontal axis*) is 700–1300 km s^{-1}, and the range in T_{mb} (vertical axis) is −100–200 mK. Coordinate axes are offsets in arcseconds from the nucleus. (*b*) Mosaic of 13 CO(2–1) line spectra, in the same format as the CO(1–0) spectra.

TABLE 10

Hα OBSERVATION LOG

Spectrum	Date	Grating (lines mm^{-1})	Dispersion (Å pixel^{-1})	Exposure (s)	Position Angle
csd09181.....	1993.12.06	1800	0.40	1800	90°
csd09184.....	1993.12.06	600	1.27	1800	90
csd09245.....	1993.12.07	1200	0.62	1282	90

The IRAM CO(2–1) line spectra indicate a steeply rising inner rotation curve, as in the Hα data (see next section and Fig. 19). This is typical of galaxies with nuclear rings as these generally occur at a maximum of the rotation curve.

8. Hα OBSERVATIONS

In order to search for possible counter-rotating ionized gas in the inner regions of NGC 7217, and also to obtain additional Hα radial velocity measurements, we observed the galaxy with the Cassegrain spectrograph of the 188 cm telescope of Okayama Observatory on 1993 December 4, 6, 7, and 8. We obtained six high-resolution spectra with gratings of 1800, 1200, or 600 lines mm^{-1}, respectively, and a 512 × 512 pixel CCD with 20 × 20 μm pixels, using a two-pixel binning in the spatial direction. The typical seeing was 2″–3″, resulting in a 1.″5 × 0.40–1.27 Å effective pixel size, depending on the grating used (Table 10). The slit position angle was either 90° or 95°, and exposure times were typically 20–30 minutes.

The spectra were reduced using standard techniques. Unfortunately, saturated comparison spectra posed a serious problem in attaining the required accuracy in the wavelength calibration of some spectra, so only three spectra were usable for a determination of Hα rotation velocities (see Table 10). These spectra were all taken at a position angle of 90°, close to the kinematic and photometric major axis derived from our other data. The heliocentric radial Hα line velocities derived from the spectra, and their estimated uncertainties, are listed in Table 11 in order of the position along the slit, together with the grating used. A binning of 2.2 pixels (3.″4) in position was used.

The data are plotted in Figure 22, where we excluded the six values determined with the 600 lines mm^{-1} grating (see Table 11), since they all have an error exceeding 40 km s^{-1}. For comparison, Figure 22 also shows the Hα velocities measured by Peterson et al. (1978) in four spectra along position angles of 90° and 86°. The Hα rotation curve of the galaxy has been determined out to about 90″ radius (see open circles in Fig. 19), and is rather flat, like those of other normal objects of similar morphological classification (see, e.g., Rubin et al. 1985).

None of our individual spectra show any sign of counter-rotating ionized gas, and neither does an averaged spectrum, nor do the Hα profiles look asymmetric, unlike the stellar absorption lines analyzed by Merrifield & Kuijken (1994). We therefore conclude that there is no sign of counter-rotation in the Hα line spectra and that the galaxy has an undisturbed rotation curve.

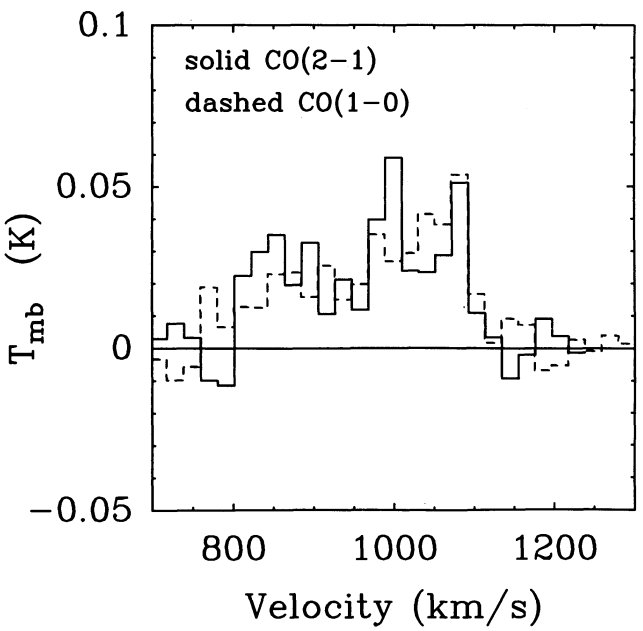

FIG. 21.—CO(1–0) spectrum (*dashed line*) and CO(2–1) spectrum (*solid line*) of the inner 26″ diameter region. These spectra are based on direct sums of the nine central spectra in each line. The velocity resolution is 5.2 and 10.4 km s^{-1} for the (1–0) and (2–1) line spectrum, and the rms noise is 10 and 13 mK, respectively.

9. MASS MODELS AND GAS SIMULATIONS

The only way to truly understand the nature of the ring patterns seen in NGC 7217 is to try to simulate its gas-dynamics. We present in this section simulations based on gas streaming in a potential derived from the KPNO near-infrared image of the galaxy, with no self-gravitation. The method used has already been described in Garcia-Burillo, Combes, & Gerin (1993).

TABLE 11

Hα ROTATION VELOCITIES

Radius	V_{hel} (km s^{-1})	Error (km s^{-1})	Grating (lines mm^{-1})
−76.″8E	815	24	1200
−72.2	804	8	1200
−31.8	817	12	1200
−28.2	828	62	600
−18.2	803	16	1200
−14.0	815	5	1800
−13.8	835	10	1200
−10.2	824	48	600
−9.4	814	7	1800
−9.2	829	7	1200
4.2	985	33	1200
7.8	1100	42	600
8.6	1091	5	1800
8.8	1080	10	1200
12.2	1076	56	600
13.0	1079	8	1800
13.2	1084	9	1200
16.8	1107	45	600
17.8	1094	16	1200
21.2	1111	78	600
26.8	1113	15	1200
49.2W.....	1114	24	1200

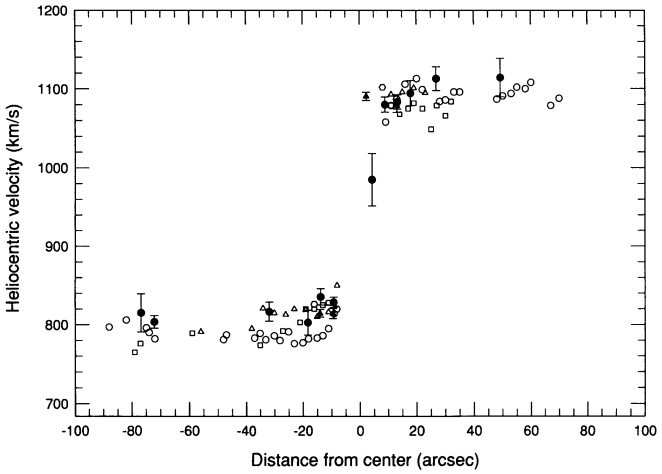

FIG. 22.—Hα emission line heliocentric velocities as a function of angular distance from the center of NGC 7217. The new Okayama data (see Tables 10 and 11) are the filled circles with error bars. The open symbols are measurements from Peterson et al. (1978); the circles represent their best quality spectrum (see their Fig. 3).

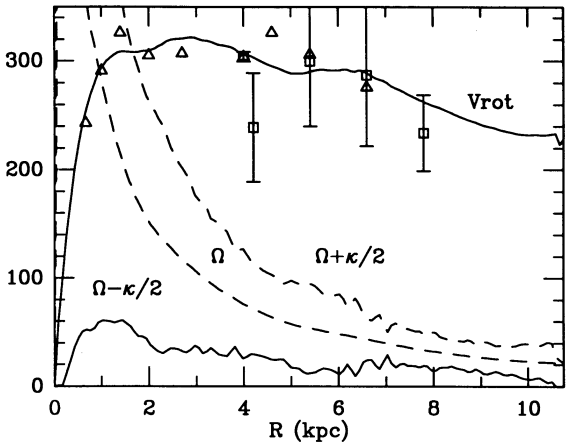

FIG. 23.—Rotation curve (*solid line*) and derived frequencies for the "maximum disk" model, with an assumed spheroid-to-disk mass ratio of 0.5. The disk is derived from the *I*-band image, with an M/L constant with radius. The triangles are the Hα rotational velocities; the squares the H I rotational velocities from Fig. 22.

9.1. *Gravitational Potential*

We use the *I*-band image, after spheroid subtraction and deprojection (see § 4.4), to determine the gravitational potential of the disk. Because of residual near-side extinction in this image, we have first symmetrized the image with respect to the origin, to minimize artificial local perturbations. The corresponding gravitational potential is computed by a Fourier transform on 256 × 256 pixels of 1.″2 × 1.″2 size, assuming a constant M/L ratio over the disk. We then add in the spheroidal component as either one or two Plummer analytical functions. We have some freedom in the respective mass-to-light ratios for the disk and spheroid, since they could be different. We have therefore run two series of simulations, corresponding to the extreme possible choices: the "maximum disk" model, where the spheroid-to-disk mass ratio is 0.5, and the "maximum bulge" model, where this ratio is 2.4, similar to the corresponding light ratio derived in § 4. We have adjusted the size and mass parameters of the various components, in order to fit the observed rotation curve. These parameters are summarized in Table 12. The rotation velocity, circular angular velocity, and Lindblad precession frequencies versus radius are shown in Figure 23 for the maximum disk model and in Figure 24 for the maximum bulge model.

TABLE 12

PARAMETERS OF THE MASS MODELS[a]

Parameter	Maximum-disk Model	Maximum-bulge Model
M_{disk} ($M_\odot$).....	6E10	3.7E10
M_{bulge} ($M_\odot$).....	3E10	9E10
M_{disk}/M_{bulge}.....	0.5	2.4
M_{b1} ($M_\odot$).....	3E10	3E10
a_{b1} (kpc).....	1	1
M_{b2} ($M_\odot$).....	0	6E10
a_{b2} (kpc).....	...	3.5
M/L_B (disk).....	8.6	5.3
M/L_B (bulge).....	1.8	5.3

[a] The analytical bulge component is composed of one Plummer for the "Max-disk" model, and two Plummers for the "Max-bulge" model (indexed *b*1 and *b*2).

The potential is extended perpendicular to the plane under the assumption of cylindrical symmetry (i.e., x and y forces independent of z), since we are concerned only with the gas component whose thickness is only a fraction of a kpc. For the z forces, we assume that the stellar plane obeys the equilibrium of an infinite layer, with a density $\rho = \rho_0\ \mathrm{sech}^2\ (z/H)$, where H is the scale height. We adopt $H = 1$ kpc.

9.2. *Numerical Method*

The hydrodynamics of the gas is simulated with the collisional model described in Combes & Gerin (1985), extended to three dimensions. We simulate a mass spectrum of 4×10^4 clouds ranging from 10^3 to $10^6\ M_\odot$ that interact via collisions (i.e., they can exchange mass or coalesce). Clouds over $3 \times 10^5\ M_\odot$ (giant molecular clouds) are dispersed by star formation after a lifetime of 4×10^7 yr, and their mass is reinjected to the interstellar medium in the form of small clouds, with a velocity dispersion of 10 km s^{-1}. The collision grid has a spatial resolution of the order of 100 pc.

Clouds are moved as test particles in the potential determined in the previous section. The potential is decomposed

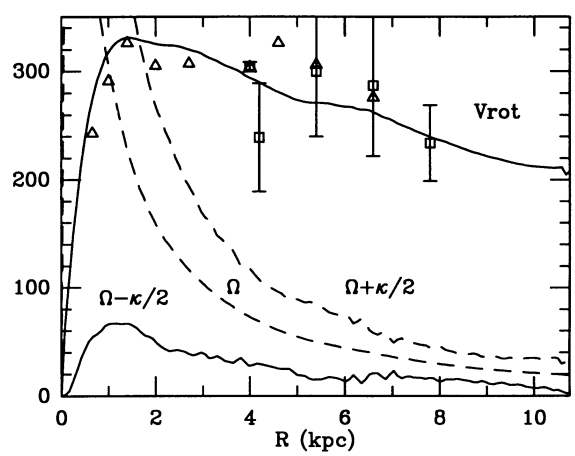

FIG. 24.—Same as Fig. 23, but for the "maximum bulge" model, where the spheroid-to-disk mass ratio is 2.4.

into its axisymmetric and nonaxisymmetric parts. Initially, the particles are launched with the rotational velocity in the axisymmetric potential, with a small velocity dispersion in the plane (10 km s^{-1}). The nonaxisymmetric perturbation is then introduced gradually, with a constant angular velocity Ω_p. This pattern speed has been varied from 40 to 80 km s^{-1} kpc^{-1} to obtain the best morphological fit with the observations.

The initial radial distribution of molecular clouds is an exponential disk of scale length $a_d = 3$ kpc. Its distribution perpendicular to the plane is Gaussian, as expected from the equilibrium of a multicomponent system, with a thickness of 50 pc. We run the simulations until a quasi-stationary state is obtained, i.e., during about 10^9 yr. Both particle plots and contour maps are produced, to better compare the final morphology to observations.

9.3. *Results*

9.3.1. *Maximum Disk Model*

The first simulations (see Fig. 25) were made with a low value of the pattern speed Ω_p with respect to the maximum of the $\Omega - \kappa/2$ curve, so that two inner Lindblad resonances (ILRs) could exist. There is then a very quick gas flow toward the center, toward the resonance region, and formation of a highly elongated nuclear ring. The behavior of the gas is well understood from the gravitational torques of the bar (see, e.g., Combes 1988). The gas flow toward the center is so large, that there is not enough gas that could be driven out toward the outer Lindblad resonance (OLR), which is located at a large radius. It can be clearly concluded that such a low pattern speed does not correspond with the observed morphology of NGC 7217 (Figs. 1–3).

We then simulated the gasdynamics with $\Omega_p = 60$, 70, and 80 km s^{-1} kpc^{-1}, which are very close to the maximum of the $\Omega - \kappa/2$ curve. The best fit is obtained with $\Omega_p = 70$ km s^{-1} kpc^{-1} (Fig. 26). In this case, an inner ring of about 2 kpc radius forms at the inner 4/1 ultraharmonic resonance (UHR), near corotation, with a characteristic squarish form; gas also accumulates in an outer ring near 5 kpc radius. The inner ring is so contrasted that there is barely any nuclear ring.

9.3.2. *Maximum Bulge Model*

The same features are found with the maximum bulge model, although the nonaxisymmetric perturbation is then much weaker. Figure 27 shows the low pattern speed case, with its conspicuous elongated nuclear ring. As for the maximum disk model, this does not compare favorably with the observed morphology of NGC 7217. Instead, the best fit is again obtained with $\Omega_p = 70$ km s^{-1} kpc^{-1} (Fig. 28). In this case, three rings can be distinguished at the approximate positions of the observed rings: 0.6, 2, and 5 kpc, corresponding to the ILR, the inner 4/1 resonance and the OLR. This plot can be directly compared with the deprojected *B* image in Figure 10.

These numerical experiments show that, *although NGC 7217 appears quite axisymmetric, the very slight $m = 2$ perturbation revealed by the Fourier analysis is sufficient to produce in the gas the characteristic ringed morphology observed.* The mechanism proposed here, based on gas accumulation at resonances, is supported by the observations: most of the star formation takes place in the rings, where atomic and molecular gas are indeed concentrated. Also, our adopted orientation parameters have effectively minimized the nonaxisymmetric components in the system. If we can obtain the rings under this circumstance, then our conclusion would be unchanged for slightly different orientation parameters, for example, like those derived from the H I kinematics, which would only increase the nonaxisymmetry.

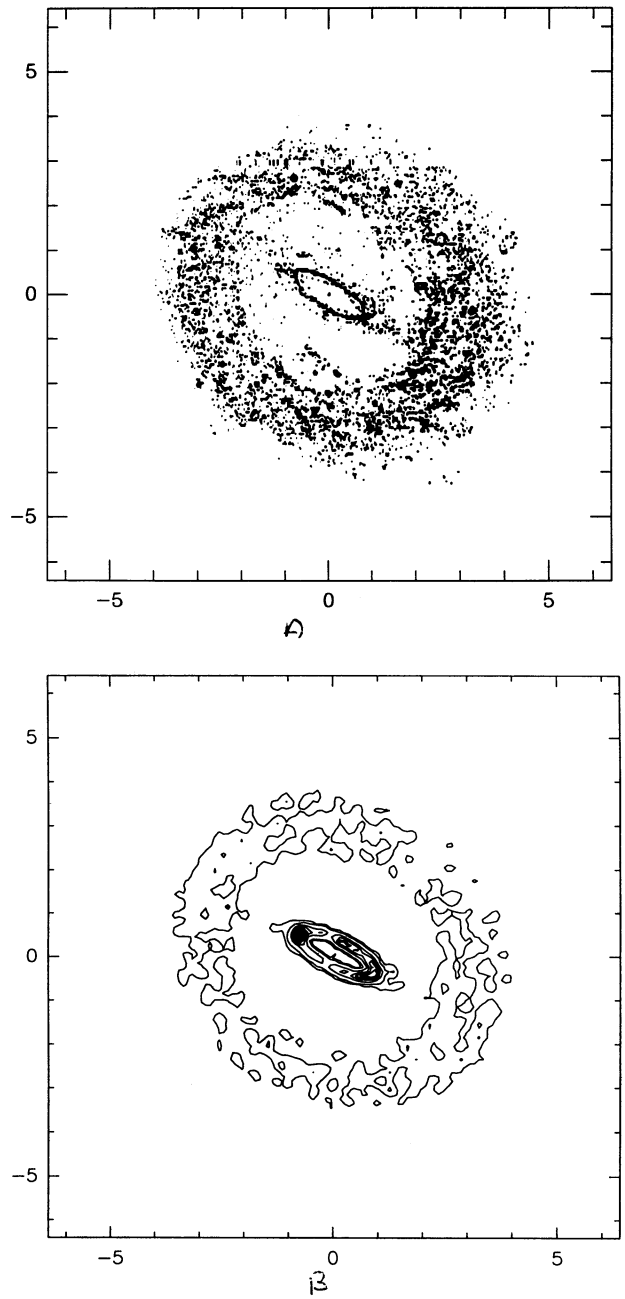

FIG. 25.—Gas behavior in the "Max-disk" mass model, with a pattern speed of 40 km s^{-1} kpc^{-1}: (*a*) particle plot, (*b*) linear contours map. Both reveal the formation of an elongated nuclear ring at ILR. The morphology is inconsistent with the observed structure in NGC 7217.

10. DISCUSSION

10.1. *NGC 7217 as a Spheroid-Dominated, Resonance Ring Spiral Galaxy*

The surprising structure of NGC 7217, with its extensive luminous outer stellar halo, its nuclear dust ring, its large spheroid-to-disk luminosity ratio, and its remarkable axisymmetry, makes it an interesting example of a ringed galaxy that,

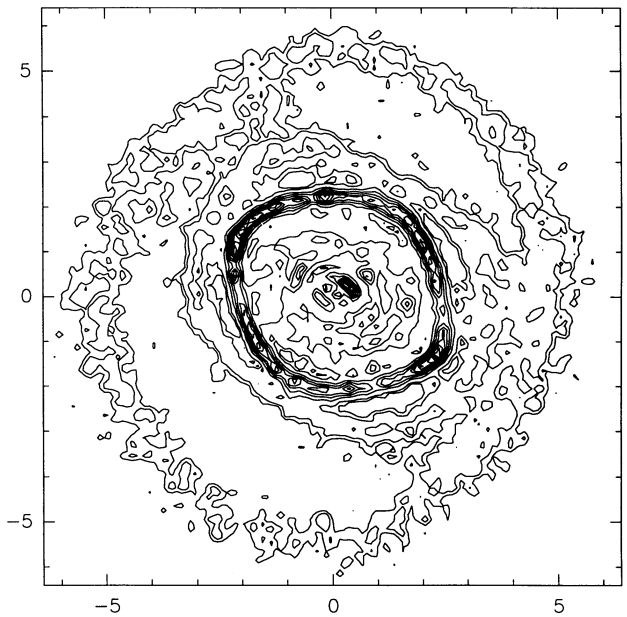

FIG. 26.—Gas behavior in the "Max-disk" mass model, with a pattern speed of 70 km s^{-1} kpc^{-1}: the contours show the presence of an inner ring at the 4/1 UHR and an outer ring at OLR, but no nuclear ring. This is also inconsistent with the structure of NGC 7217.

at least at first sight, does not readily fit into ideas deduced from other, less axisymmetric galaxies. The appearance of NGC 7217 is similar to other galaxies with known large spheroid-to-disk ratios. The first case that comes to mind is the Sombrero galaxy, NGC 4594 (see Sandage 1961), which is viewed only 6° from edge-on. The flocculent structure of the disk in blue light is nevertheless clear and may even be ringlike. According to Hamabe (1982), the *B*-band spheroid-to-disk ratio of NGC 4594 is 3.7. Another example of a spheroid-dominated spiral is NGC 3928. This galaxy is classified as E0 in RC2, but a high-quality CFHT plate published by van den Bergh (1980) revealed a very small, tightly wrapped spiral in the inner regions. Surface photometry by Taniguchi & Watanabe (1987) yielded a *B*-band spheroid-to-disk ratio of 3.0 for this galaxy. Both galaxies are more spheroid-dominated than NGC 7217 but they all have in common a tightness or flocculence of the spiral structure and little or no evidence for a bar or oval. However, the spiral in NGC 3928 is intrinsically much smaller than those in NGC 7217 or 4594. Finally, Rubin et al. (1978) suggested that the peculiar one-armed spiral, NGC 4378, would probably resemble NGC 4594 if it were seen edge-on. The excellent photograph in their Figure 1 shows that NGC 4378 is inclined about the same as NGC 7217 and, apart from the single-arm morphology, very much resembles NGC 7217.

Thus, we see that NGC 7217 is not without precedent, that other similar galaxies do exist. Our numerical simulations have shown that the three ring features in NGC 7217 are likely to be associated with the same resonances thought to be associated with the typical inner, outer, and nuclear rings seen in normal barred spirals. These interpretations are further supported by size ratios of the observed rings in NGC 7217. The ratios of the diameters are $d(R)/d(rs) = 2.4$, $d(R)/d(\text{stellar nr}) = 7.2$, and $d(R)/d(\text{dust nr}) = 9.0$. The ratio of the inner and outer ring diameters is very similar to the ratio, 2.2, observed for the same kinds of features in galaxies with clear bars and ovals

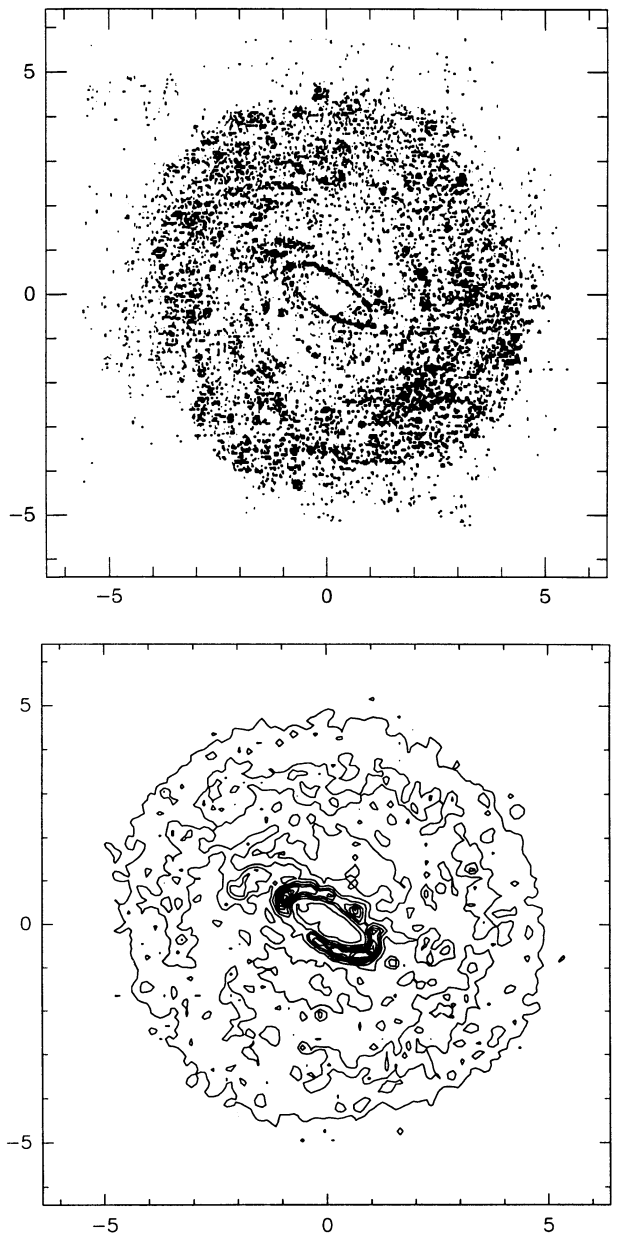

FIG. 27.—Same as Fig. 25, but for the "Max-bulge" mass model, with a pattern speed of 40 km s^{-1} kpc^{-1}.

(Athanassoula et al. 1982; Buta 1986a, 1995). It has been suggested that this ratio is roughly expected if outer rings are associated with the OLR and inner rings are associated with the inner 4/1 ultraharmonic resonance near corotation. The nuclear rings could be associated with an inner Lindblad resonance.

If the rings of NGC 7217 represent the usual resonances found in other spiral galaxies, what is the material in the rings resonating with? Figure 10 (*lower right panel*) suggests that a weak oval distortion may be present in the stellar disk component. It is well-known that ovals need not be particularly prominent to be capable of driving spirals or rings (see, e.g., Schwarz 1981, 1984; Combes & Gerin 1985). The only requirement is that the forcing due to the oval be strong enough to cause periodic orbits to cross near resonances, so that gas is

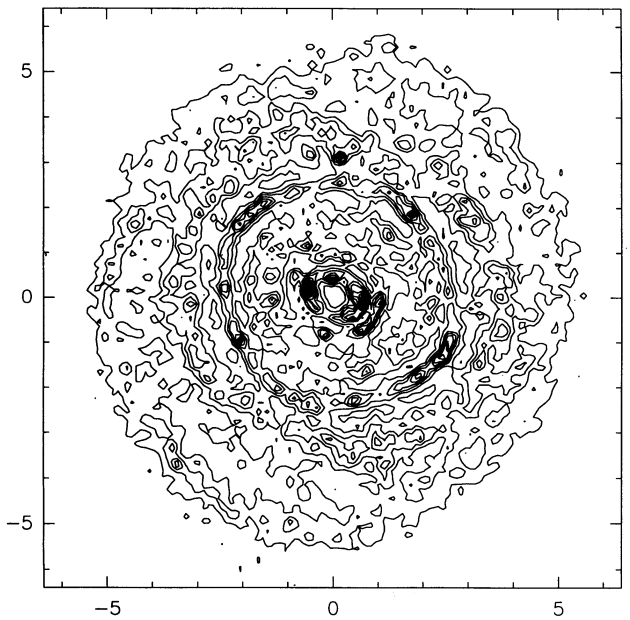

FIG. 28.—Same as Fig. 26, but for the "Max-bulge" mass model, with a pattern speed of 70 km s^{-1} kpc^{-1}. Of all of the models tried, this one provides the closest approximation to the observed structure of NGC 7217.

gathered into some of these orbits. If this is indeed the reason for the rings in NGC 7217, then it would underscore how even the most axisymmetric-appearing galaxies must have some kind of nonaxisymmetry that helps to drive their structure.

The delineation of the inside edge of the stellar nuclear ring by a narrow dust lane is very similar to what has been observed in the strongly barred galaxy NGC 4314. This galaxy also has a prominent optical, star-forming nuclear ring, corresponding to the inner Lindblad resonance of the bar. A sharp dust lane defines the inner side of this ring (Benedict et al. 1992), and the molecular cloud ring also peaks just inside the radio-continuum emission tracing the optical ring (Combes et al. 1992). This was interpreted by Combes et al. (1992) as evidence of evolution of the ring, slowly decreasing in radius by dynamical friction and dissipation, which occurs when there is not enough gas left in the galaxy disk between corotation and ILR to replenish the nuclear ring. This is the case in NGC 4314, a very H I poor system. Since NGC 7217 is also very poor in H I inside the outer ring, it is probable that the nuclear dust ring owes its origin to the same process.

10.2. *The Nature of the Counter-Rotating Stars*

The counter-rotating stars in NGC 7217, discovered by Merrifield & Kuijken (1994), could have something to do with the large spheroidal component in the galaxy. In attempting to evaluate all alternative possibilities to these stars being truly counter-rotating disk stars, these authors considered that a slow rotating, large-dispersion bulge component could explain the extended "tail" of the absorption line profiles along the major axis. They suggest that the bulge would have to contribute an almost constant 60% of the light between 10″ and 60″ radius. The decomposition parameters in Table 5 can be used to evaluate this. We find that in blue light, the ratio of the bulge plus halo surface brightness to the total surface brightness exceeds 50% for all radii less than 60″, and reaches a minimum of 37% near 80″ (the radius of the outer ring). The relative spheroid contribution predicted by the decomposition is uniform at about 55% in the radius range 30″–60″. At smaller radii than 30″, the spheroid contribution increases and the ratio approaches 1 as the radius approaches zero. In *V* and *I*, the spheroid contribution will be larger than in *B* at all radii. Thus, the spheroidal component in NGC 7217 may indeed be as important as Merrifield and Kuijken deduced that it would have to be in order to explain their line profile observations.

Merrifield and Kuijken interpreted the *r*-band luminosity profile of NGC 7217 (Kent 1986) in a very different manner. They believe that the change in slope of the profile near $\approx 10''$ radius indicates that the disk dominates beyond this radius (see their Fig. 2). However, this deduction is not based on a formal decomposition and forces the bulge to truncate completely near 20″ radius. Also, it is clear that the disk model these authors adopted will not extrapolate reliably beyond the outer ring and explain the shallower luminosity gradient found out there.

Although the bulge of NGC 7217 may be more important than Merrifield and Kuijken believed, it is not clear that this can explain the secondary peak they found in the velocity distribution at the negative circular speed. They believe that, because the fraction of counter-rotating stars contributing to the line of sight velocity dispersion remains nearly constant outside 10″ radius, the counter-rotating stars cannot be bulge stars. A truly nonrotating bulge or spheroidal component should produce a secondary peak near the systemic velocity. A small oppositely directed net rotation of the bulge could produce an offset secondary peak, but since the bulge would be expected to have a larger velocity dispersion than the disk stars this would perhaps only add a long tail to the line-of-sight velocity dispersion. Nevertheless, if our results are correct, the role of the bulge should be reconsidered in the analysis of absorption-line profiles in the inner regions of the galaxy.

10.3. *The Effects of Internal Absorption in the Disk Component*

Thus far we have not considered the effects of internal absorption in the disk component of NGC 7217 on our model of the system. Such absorption is obvious on the near side of the system, and of course it is very clear in the Sombrero galaxy. In the case of NGC 3928, Taniguchi & Watanabe (1987) have interpreted a "dip" in the luminosity profile, found in the region where the miniature spiral is observed, as due to absorption of the light of the much more extended spheroidal component by extinction in the miniature disk. The dip is more prominent at longer wavelengths because the contribution from young stars is reduced at these wavelengths. In the context of a simple two-component model, we would expect that if the disk of NGC 7217 is optically thick we should see a similar dip and therefore a more humped profile than is actually seen, if the disk extinction does not extend well beyond the outer ring. Based on a study of overlapping pairs of galaxies where a spiral appears projected against a background elliptical, White & Keel (1992) deduced that disks are probably locally optically thick in regions of active star formation, such as in spiral arms, and are optically thin between arms. Thus, we expect that NGC 7217 is most optically thick in the outer ring region, a region which was excluded from our decompositions. Still, the effects of internal absorption cannot be ignored, and could be best evaluated with *H*- or *K*-band images.

10.4. *The Formation of Spheroid-Dominated Spiral Galaxies*

Finally, the formation of large spheroid disk galaxies is an important problem. In the case of NGC 3928, Taniguchi &

Watanabe (1987) suggest that the gas in the small inner spiral was acquired from the outside. This may be a plausible interpretation in that case, because the spiral part has a very low luminosity and the galaxy is a member of a nearby group. However, NGC 7217 is largely isolated, so that another interpretation may be warranted. The barlike distortion that we see in the near-infrared image may be strong enough to cause the rings in NGC 7217, but it may also have been stronger in the past since gas mass accretion toward the center can destroy a bar, as has been shown by Hasan & Norman (1990) and Pfenniger & Norman (1990). This destruction of the bar is accompanied by a reinforcing of the bulge, which may have been very effective in NGC 7217. Identification and further study of other examples should shed much-needed light on the problems of these galaxies.

11. CONCLUSIONS

Our main findings from this study are as follows:

1. The inner zone of flocculent spiral structure and rings in NGC 7217 is surrounded by an extensive luminous stellar halo with nearly circular isophotes. This halo could merely be the light of the bulge at large radii, or it could be genuinely distinct from the bulge. Since this light extends to nearly 3 times the radius of the outer ring, this would mean that NGC 7217 is a very "spheroid-dominated" galaxy. This is confirmed by a standard $r^{1/4}$ spheroid and exponential disk decomposition model of the luminosity profiles, which indicates that the spheroid contributes about 70% of the total *B*-band luminosity. The spheroid-to-disk luminosity ratio derived is about 2.3, one of the largest known among ordinary galaxies. If the bulge and stellar halo are truly distinct, then we would expect the bulge to be rapidly rotating while the halo would be slowly rotating, and we would also expect the halo to be very metal poor compared to the bulge. We cannot make this distinction at the present time, except to note that the color gradients in the galaxy are fairly small and not unusual.

2. The outer ring of NGC 7217 is the locus of most of the H I gas and recent star formation in the galaxy. The net colors of this feature are as blue as the integrated colors of late-type spirals and irregulars. There is a weak but clear old component to the ring, indicating that it has been a site of enhanced star formation for a long time. The ring, though prominent in direct images, includes only 4.4% of the total *B*-band luminosity.

3. Fourier analysis of the intensities in the *I* band reveal a tightly wrapped two-armed stellar spiral in the region of the outer ring and a possible weak oval distortion. The spiral is trailing with respect to the rotation of the neutral and ionized gas. Since the Fourier analysis used orientation parameters that essentially minimized any contribution of the outer ring to the nonaxisymmetric component of the potential, and also which disagree with the best-fitting parameters derived from H I kinematics, it is likely that any oval distortion in NGC 7217 has an amplitude and phase which differs somewhat from what we have found.

4. An extended distribution of molecular hydrogen gas is found in the region of the nuclear ring. Tentative detection of CO is also made at points near the positions of the inner and outer rings.

5. The Hα rotation curve is relatively normal for the Hubble type of NGC 7217. The H I rotation curve covers only the outer ring and does not extend the rotational information beyond the optical disk. No evidence is found for counter-rotation in the ionized gas.

6. Mass models deduced from the *I*-band light distribution suggest that the rings in NGC 7217 are normal resonance rings similar to those observed in more obviously barred galaxies. It is apparently possible for even the weakest perturbation to generate gaseous rings near resonances. However, the rings in NGC 7217 are intrinsically much more circular than the rings normally seen in SB galaxies.

We suggest that the counter-rotating stars discovered by Merrifield & Kuijken (1994) could be associated in some way with the large spheroidal component in NGC 7217. This makes the galaxy a particularly important object in which to search for globular clusters.

We wish to thank A. Coolen and P. S. Mulder for their help in preparing the Westerbork maps, M. Hamabe, and S. Yoshida for their help in obtaining and reducing the CCD images at Kiso Observatory, and G. B. Purcell for help in obtaining the KPNO CCD images. We also would like to thank the Okayama staff for their support with the Okayama spectral observations. An anonymous referee made many helpful suggestions which improved the quality of this paper, for which we are grateful. We also thank D. A. Crocker for a helpful comment. IRAF is distributed by the National Optical Astronomy Observatories, which is operated by the Association of Universities for Research in Astronomy, Inc. (AURA), under cooperative agreement with the US National Science Foundation. We have made use of the NASA/IPAC Extragalactic Database (NED), which is operated by the Jet Propulsion Laboratory, California Institute of Technology, under contract with the US National Aeronautics and Space Administration. The Westerbork Radio Observatory is operated by the Netherlands Foundation for Research in Astronomy (NFRA/ASTRON) with financial support from the Netherlands Organization for the Advancement of Research (NWO). W. v. D. gratefully acknowledges the financial support of the Meudon Observatory during his visits. R. B. gratefully acknowledges the support of NSF EPSCoR grant RII8996152 and NSF grant AST 90-14137 to the University of Alabama.

APPENDIX

The error bars in the profiles in Figure 7, and in Tables 3 and 4, were computed as follows. First, we computed errors in the surface brightness level of each point on the profiles. This error includes the counting statistics, the readout noise, the gain, and the uncertainty in the sky level. If N_R is the read noise in electrons per second, g is the gain in electrons per ADU, and N is the number of ADU in a given pixel, then the noise in that pixel is given by

$$\sigma_1(N) = \frac{\sqrt{gN + N_R^2}}{g} \tag{A1}$$

(see IRAF documentation). Each isophote that was fitted, however, is defined by a large number of individual pixels, so that the uncertainty in the level is much less than given by equation (1). To approximate this uncertainty, we computed the circumference C of each ellipse in pixels of the original array (even if the ellipse fit was made to an isophote obtained with a binned array). Then we computed

$$\sigma(N) = \frac{\sigma_1(N)}{\sqrt{C}} . \tag{A2}$$

For the uncertainty in the sky level S, in ADU, we set $\sigma(S) = xS$, where $x = 0.001$ for the KPNO B and V images and for the Kiso images, and 0.003 for the KPNO I image. Then the uncertainty in the surface brightness level μ (mag arcsec^{-2}) was derived from

$$\sigma(\mu) = \sqrt{\sigma_0^2 + \left(\frac{1.0857}{\Delta N}\right)^2 [\,\sigma(N)^2 + \sigma(S)^2]} , \tag{A3}$$

where σ_0 is the zero point error from the standard star transformations for the KPNO images, or aperture photometry for the Kiso images, and $\Delta N = N - S$ is the net count associated with the level. Since we chose surface brightness levels, and our ellipse-fitting program returned a semimajor radius a, we have transformed the uncertainty $\sigma(\mu)$ into $\sigma(a)$ using

$$\sigma(a) = \left(\frac{\partial \mu}{\partial a}\right)^{-1} \sigma(\mu) . \tag{A4}$$

These results as illustrated in Figure 7 show that the Kiso and KPNO V-band profiles are significantly different at about the 1 σ level at $a = 195''$. The error bars do not account for significant departures of an isophote from an elliptical shape, any residual contaminating effects of field objects, or possible scattered light, and thus are probably underestimates.

For the color index profiles in Figure 7, we computed the errors as

$$\sigma(B-V) = \sqrt{\sigma_0(B-V)^2 + \sigma(B)^2 + \sigma(V)^2} , \tag{A5}$$

where $\sigma_0(B-V)$ is the zero point error for the $B-V$ transformations and $\sigma(B)$ and $\sigma(V)$ are the uncertainties in the individual profiles (computed from eq. [3], but without the individual filter zero point errors taken into account). Similar relations were used for $V-R$ and $V-I$. We show the error bars for the color index rather than the radius since the radius errors are less meaningful for these profiles.

REFERENCES

Allen, R. J., Ekers, R. D., & Terlouw, J. P. 1985, in Proc. Internat. Workshop on Data Analysis in Astronomy at Erice, ed. V. di Gesu (London: Plenum), 271
Athanassoula, E., Bosma, A., Créze, M., & Schwarz, M. P. 1982, A&A, 107, 101
Balkowski, C., & Chamaraux, P. 1983, A&AS, 51, 331
Begeman, K. 1989, A&A, 223, 47
Benedict, G. F., Higdon, J. L., Tollestrup, E. V., Hahn, J. M., & Harvey, P. M. 1992, AJ, 103, 757
Boroson, T. 1981 ApJS, 46, 177
Bosma, A. 1981, AJ, 86, 1791
Bottinelli, L., Gouguenheim, L., & Paturel, G. 1980a, A&A, 88, 32
Bottinelli, L., Gouguenheim, L., Paturel, G., & de Vaucouleurs, G. 1980b, ApJ, 242, L153
———. 1983, A&A, 118, 4
Braine, J. 1992, Ph.D. thesis, Univ. Paris
Braine, J., & Combes, F. 1992, A&A, 264, 433
Braine, J., Combes, F., Casoli, F., Dupraz, C., Gérin, M., Klein, U., Wielebinski, R., & Brouillet, N. 1993, A&AS, 97, 887
Buta, R. 1986a, ApJS, 61, 609
———. 1986b, ApJS, 61, 631
———. 1990, ApJ, 356, 87
———. 1991, in IAU Symp. No. 146, Dynamics of Galaxies and Their Molecular Cloud Distributions, ed. F. Combes & F. Casoli (Dordrecht: Kluwer), 251
———. 1995, ApJS, 96, 39
Buta, R., & Crocker, D. 1991, AJ, 102, 1715
———. 1992, AJ, 103, 1804
Buta, R., de Vaucouleurs, G., Mitra, S., & Corwin, H. G. 1994, AJ, 107, 118
Buta, R., & Williams, K. L. 1995, AJ, 109, 543
Cawson, M. 1983, Ph. D. thesis, Cambridge Univ.
Combes, F. 1988, in Galactic and Extragalactic Star Formation, ed. R. E. Pudritz & M. Fich (Dordrecht: Kluwer), 475
Combes, F., & Gerin, M. 1985, A&A, 150, 327
Combes, F., Gerin, M., Nakai, N., Kawabe, R., & Shaw, M. A. 1992, A&A, 259, L27
Condon, J. J. 1987, ApJS, 65, 485
Cornell, M., Aaronson, M., Bothun, G., & Mould, J. 1987, ApJS, 64, 507
Davies, L. E., & Seaquist, E. R. 1983, ApJS, 53, 269
Davis, L. E., Cawson, M., Davies, R. L., & Illingworth, G. 1985, AJ, 90, 169
de Vaucouleurs, G. 1958, ApJ, 127, 487
———. 1959, Handbuch Phys., 53, 275
———. 1975, ApJS, 29, 193
de Vaucouleurs G., & Buta, R. J. 1980 AJ, 85, 637
de Vaucouleurs, G., de Vaucouleurs, A., & Corwin, H. 1976, Second Reference Catalogue of Bright Galaxies (Austin: Univ. Texas Press) (RC2)
de Vaucouleurs, G., de Vaucouleurs, A., Corwin, H., Buta, R., Paturel, G., & Fouqué, P. 1991, Third Reference Catalogue of Bright Galaxies (New York: Springer) (RC3)
de Vaucouleurs, A., & Longo, G. 1988, Univ. Texas Monographs in Astronomy no. 5
Forbes, D. A. 1992, A&AS, 92, 583
Garcia-Burillo, S., Combes, F., & Gerin, M. 1993, A&A, 274, 148
Gilmore, G., King, I., & van der Kruit, P. 1989, The Milky Way as a Galaxy (Mill Valley: University Science Books)
Gioia, I. M., & Fabbiano, G. 1987, ApJS, 63, 771
Giovanelli, R., & Haynes, M. P. 1985, AJ, 90, 2445
Giovanelli, R., Haynes, M. P., Rubin, V. C., & Ford, W. K. 1986, ApJ, 301, L7
Hamabe, M. 1982, PASJ, 34, 423
Hasan, H., & Norman, C. A. 1990, ApJ, 361, 69
Hewitt, J. N., Haynes, M. P., & Giovanelli, R. 1983, AJ, 88, 272
Högbom, J. A. 1974, A&AS, 15, 417
Huchtmeier, W. K., & Richter, O.-G. 1989, A General Catalog of H I Observations of Galaxies (New York: Springer)
Hummel, E. 1981, A&A, 93, 93
Hummel, E., van der Hulst, J. M., Keel, W. C., & Kennicutt, R. C. 1987, A&AS, 70, 517
Kalnajs, A. 1983, in IAU Symp. 100, Internal Kinematics and Dynamics of Galaxies, ed. E. Athanassoula (Dordrecht: Reidel), 87
Karachentseva, I. 1973, Comm. Special Astrophys. Obs. USSR, 8, 1
Kent, S. M. 1986, AJ, 91, 1301
Kuijken, K. 1993, PASP, 105, 1016
Landolt, A. 1992, AJ, 104, 340
Longo, G., & de Vaucouleurs, A. 1983, Univ. Texas Monographs in Astronomy no. 3
Merrifield, M., & Kuijken, K. 1994, ApJ, 432, 575
Mulder, P. S., & van Driel, W. 1993, A&A, 272, 63
Paturel, G., Bottinelli, L., Gouguenheim, L., & Fouqué, P. 1990, Catalogue of H I Data (Paris: Obs. Lyon and Paris-Meudon)
Peterson, C. J., Rubin, V. C., Ford, W. K., & Roberts, M. S. 1978, ApJ, 226, 770
Pfenniger, D., & Norman, C. A. 1990, ApJ, 363, 391
Press, W. H., Flannery, B. P., Teukolsky, S. A., & Vetterling, W. T. 1988, Numerical Recipes (Cambridge: Cambridge Univ. Press)
Pogge, R. W. 1989, ApJS, 71, 433
Rubin, V. C., Burstein, D., Ford, W. K., & Thonnard, N. 1985, ApJ, 289, 81

Rubin, V. C., Ford, W. K., Strom, K. M., Strom, S. E., & Romanishin, W. 1978, ApJ, 224, 782
Rubin, V. C., Graham, J. A., & Kenney, J. 1992, ApJ, 394, L9
Sandage, A. 1961, The Hubble Atlas of Galaxies, Carnegie Inst. Washington Pub. no. 618
Sandage, A., & Tammann, G. 1981, A Revised Shapley-Ames Catalog of Bright Galaxies, Carnegie Inst. Washington Pub. no. 635 (RSA)
Schwarz, M. P. 1981, ApJ, 247, 77
———. 1984, MNRAS, 209, 93
Scoville, N. Z., & Young, J. S. 1983, ApJ, 265, 148
Simien, F., & de Vaucouleurs, G. 1986, ApJ, 302, 564
Stetson, P. B. 1987, PASP, 99, 191
Strong, A. W., et al. 1988, A&A, 207, 1
Taniguchi, Y., & Watanabe, M. 1987, ApJ, 313, 89
van den Bergh, S. 1980, PASP, 92, 409
van der Hulst, J. M., Terlouw, J. P., Begeman, K., Zwitser, W., & Roelfsema, P. R. 1992, in ASP Conf. Ser. 25, Astronomical Data Analysis and Software I, ed. D. M. Worall, C. Beimesderfer, & J. Barnes (San Francisco: ASP), 131
van Driel, W., & Buta, R. J. 1991, A&A, 245, 7
van Driel, W., & van Woerden, H. 1991, A&A, 243, 71
———. 1994, A&A, 286, 395
Verter, F. 1987, ApJS, 65, 555
Warner, P. J., Wright, M. C. H., & Baldwin, J. E. 1973, MNRAS, 63, 163
White, R. E., & Keel, W. C. 1992, Nature, 359, 129
Whitmore, B. C., & Kirschner, R. P. 1982, AJ, 87, 500
Young, J. S., & Knezek, P. M. 1989, ApJ, 347, L55
Young, J. S., Xie, S., Kenney, J. D. P., & Rice, W. L. 1989, ApJS, 70, 699
Zinn, R. 1985, ApJ, 293, 424